UNFOLDING THE CUSP-CUSP BIFURCATION OF PLANAR ENDOMORPHISMS

BERND KRAUSKOPF[†], HINKE M. OSINGA[†], AND BRUCE B. PECKHAM[§]

FINAL DRAFT of 11 October 2006

Abstract. In many applications of practical interest, for example, in control theory, economics, electronics and neural networks, the dynamics of the system under consideration can be modelled by an endomorphism, which is a discrete smooth map that does not have a uniquely defined inverse; one also speaks simply of a noninvertible map. In contrast to the better known case of a dynamical system given by a planar diffeomorphism, many questions concerning the possible dynamics and bifurcations of planar endomorphisms remain open.

In this paper we make a contribution to the bifurcation theory of planar endomorphisms. Namely we present the unfoldings of a codimension-two bifurcation, which we call the cusp-cusp bifurcation, that occurs generically in families of endomorphisms of the plane. The cusp-cusp bifurcation acts as an organising center that involves all relevant codimension-one bifurcations. The central singularity involves an interaction of two different types of cusps. Firstly, an endomorphism typically folds the phase space along curves J_0 where the Jacobian of the map is zero. The image J_1 of J_0 may contain a cusp point, which persists under perturbation; the literature also speaks of a map of type (Z_1–Z_3–Z_1). The second type of cusp occurs when a forward invariant curve W, such as a segment of an unstable manifold, crosses J_0 in a direction tangent to the zero eigenvector. Then the image of W will typically contain a cusp. This situation is of codimension one and the cusp generically evolves into a loop under perturbation. The central singularity that defines the cusp-cusp bifurcation is, hence, defined by a tangency of an invariant curve W with J_0 at the pre-image of the cusp point on J_1.

We study the bifurcations in the images of J_0 and the curve W in a neighborhood of the parameter space of the organizing center — where both images have a cusp at the same point in the phase space. To this end, we define a suitable notion of equivalence that distinguishes between the different possible local phase portraits of the invariant curve relative to the cusp on J_1. Our approach makes use of local singularity theory to derive and analyze completely a normal form of the cusp-cusp bifurcation. In total we find eight different two-parameter unfoldings of the central singularity. We illustrate how our results can be applied by showing the existence of a cusp-cusp bifurcation point in an adaptive control system. We are able to identify the associated two-parameter unfolding for this example and provide all topologically different phase portraits.

Key words. Discrete-time system, noninvertible planar map, invariant curve, unstable manifold, codimension-two bifurcation.

AMS subject classifications. 37D10, 37M20, 65P30.

1. Introduction. Many situations of practical interest are modelled mathematically by a map on a suitable phase space. In this case time is thought to be discrete and the time evolution of an initial point is given by the iterates of the map. We consider here the case that the dynamics is generated by an *endomorphism*, that is by a smooth map that does not have a (uniquely defined) inverse. As is common in the literature, we simply speak of a noninvertible map. Note that the theory of endomorphisms of the real line is well developed, with the logistic map being the most famous example. However, much less is known about the possible dynamics and bifurcations of endomorphisms on $\mathbb{R}^n$ for $n \geq 2$. We are concerned here with the case of a noninvertible planar map that maps $\mathbb{R}^2$ to itself. Such maps arise naturally as models in several areas of application, including control theory [1, 8, 9], economics

[†]Bristol Centre for Applied Nonlinear Mathematics, Department of Engineering Mathematics, University of Bristol, Bristol BS8 1TR, UK.

[§]Department of Mathematics and Statistics, University of Minnesota Duluth, Duluth, MN 55812, USA.

[2, 3], radiophysics [22] and neural networks [29]. Noninvertibility easily occurs in applications that feed back sampled data using too large a sampling time. This is effectively equivalent to the case that a vector field model is integrated with a too large integration step [21].

In a region where a planar endomorphism has a well-defined branch of an inverse it may display all the dynamical complexity of a planar *diffeomorphism*, that is, of a smooth planar map with a smooth inverse. As is now well known, planar diffeomorphisms typically show complicated dynamics, including chaos; see, for example, [13, 27] as entry points to the extensive literature. Famous examples of planar diffeomorphisms are the Hénon map [16] and the Ikeda map [17], as well as Poincaré maps of periodically driven systems, such as the forced pendulum, Van der Pol and Duffing oscillators [13, 31].

The main question in the study of planar endomorphisms is what extra dynamical features may occur beyond what is known for planar diffeomorphisms. While there have been quite a number of studies of specific planar endomorphisms, much less is known about the generic dynamics and bifurcations of planar endomorphisms that must be expected in a typical example. In short, there is, as yet, no systematic bifurcation theory for planar endomorphisms.

To be specific, consider a family of endomorphisms of the plane

$$\begin{aligned} f : \mathbb{R}^2 \times \mathbb{R}^m &\to \quad \mathbb{R}^2 \\ (x, \lambda) \quad &\mapsto f(x, \lambda) \end{aligned} \tag{1.1}$$

where $\lambda \in \mathbb{R}^m$ is an m-dimensional parameter, and f is a smooth map. We consider the case that f is not a diffeomorphism, which means that the Jacobian Df of f has a nonzero kernel. We define the (non-empty) *singular locus*

$$J_0 := \ker(Df) = \left\{ x \in \mathbb{R}^2 \mid Df\,(x) \text{ is singular} \right\}. \tag{1.2}$$

The image $J_1 := f(J_0)$ is called the *critical locus*. In the literature the critical locus J_1 is also referred to as *critical curve* [26] or *Ligne Critique* (LC) [24], while J_0 is also referred to as the *curve of merging pre-images* [26] or LC^{-1} [24]. Technically, $LC \subset J_1$ and $LC^{-1} \subset J_0$, but for this paper it is sufficient to consider them equal. This is justified by their following properties, which follow immediately from the implicit function theorem.

Proposition 1.1 (Generic properties of J_0 and J_1). *Generically, that is, for a generic family f and parameter λ in general position, the singular locus J_0 is a smooth curve where* $\dim(\ker(Df)) = 1$. *The eigenvector of the eigenvalue* 0 *is transverse to J_0 except at isolated points, called pre-cusp points, where it is tangent to J_0. Therefore, the critical locus J_1 consists of smooth curve segments that meet at isolated cusp points, which are the images of the pre-cusp points.*

Generally speaking, noninvertibility gives rise to regions with different numbers of inverses. The critical locus J_1 divides the phase plane $\mathbb{R}^2$ into regions with a constant number of pre-images. These regions are usually labeled by Z_k, where k is the number of pre-images in that region [10, 24]. Generically, that is, except at the cusp points, the map f folds the phase plane along a smooth curve in J_0, which is mapped to J_1. Therefore, the number of pre-images differs locally by two on either side of J_1 [4]. As one moves from one region into the next by crossing a fold curve the number of pre-images changes to $k \pm 2$.

In the interior of a region Z_k for $k \geq 1$ one can select a single branch of the inverse, so that the map f is locally a diffeomorphism. New phenomena, which do not occur for diffeomorphisms, may arise when a (forward) invariant object, such as a fixed point, periodic orbit or invariant manifold, interacts with the boundary of the region of definition of the inverse branch. Therefore, the bifurcation theory of endomorphisms can be thought of as the study of the interaction of dynamical objects and their images with J_0 and J_1, respectively.

The literature on noninvertible planar maps consists largely of case studies in specific examples that reveal specific phenomena and a number of codimension-one bifurcations. A lot of attention has been devoted to the structure of basins of attraction. Because a basin may consist of disconnected regions or be multiply connected, it is often referred to as a 'sea' with possibly 'islands' in it, or as 'land' with 'lakes' [18, 24]; connectivity properties are characterised with an 'island number' or 'lake number' [24]. However, as was shown in [6, 7], changes to the basin boundary are due to just two types of tangencies, called an inner and an outer tangency, of a stable set (the generalization of the stable manifold of a saddle point) with J_1.

Another topic that received a lot of interest as typical for noninvertible maps are self-intersections and associated 'loops' of (forward) invariant sets; see [10, 11, 23, 25] and [21], where loops are referred to as 'antennae'. The main interest is in bifurcations leading to the destruction of an invariant curve (also called 'IC' or 'torus'), which is sometimes the closure of the unstable manifolds of a suitable periodic orbit. To define an unstable manifold of an endomorphism consider a generic saddle point p of f (or a suitable iterate of f). Genericity of p means in particular that $p \notin J_0$. Therefore, there exists the local unstable manifold $W^u_{loc}(p)$ associated with the unique inverse branch that fixes p. The *global unstable manifold* $W^u(\mathbf{x}_0)$ can then be defined as

$$W^u(p) = \bigcup_{n=1}^{\infty} f^n(W^u_{loc}(p)). \tag{1.3}$$

Note that forward images under f are unique, so that $W^u(p)$ is indeed forward invariant. Furthermore, $W^u(p)$ is generically an immersed manifold; see, for example, [30]. Even though $W^u(p)$ may have structurally stable transverse self-intersections, it is justified to speak of $W^u(p)$ as the global unstable manifold. In particular, $W^u(p)$ can be computed numerically by any algorithm that works for diffeomorphisms; see also [6, 7]. Indeed, depending on how an unstable manifold or other invariant curve crosses J_0, a loop in its image may be the result. The codimension-one bifurcation that creates a small loop was analysed in [10, 11, 23]; we refer to it as the *loop-creation bifurcation* and it is discussed in more detail in Sec. 2. Due to forward invariance, an infinite number of loops is created in the loop-creation bifurcation, which may give rise to a rather spectacular loss of smoothness of an invariant curve. In combination with other mechanisms (as known for diffeomorphisms) of the break-up of tori, one finds phenomena such as the 'appearance of loops on an unstable manifold, and the reappearance of an attractor, this time chaotic with loops' [11, p. 107]; this type of attractor has been called a 'weakly chaotic ring' [10, 25].

In this paper we make a contribution to the bifurcation theory of planar endomorphisms by providing the first unfolding of a codimension-two bifurcation, which we call the *cusp-cusp bifurcation*. Our study was motivated by the properties of a well-referenced example of a noninvertible system, namely the discrete-time adaptive control system discussed in [1, 8, 9]. More specifically, in [10] a loop of the unstable manifold of a saddle point is found that surrounds a cusp point C_1 on J_1. Several

other codimension-one bifurcations are found near this situation, including a loop-creation bifurcation and the passing of the invariant curve through the cusp point. These bifurcations and the generic phase portraits near them are illustrated in [10] near the cusp point C_1 on J_1 as well as near the pre-cusp point C_0 on J_0, where $f(C_0) = C_1$. We identify the cusp-cusp bifurcation as the organising center of the observed dynamics in the sense that the known codimension-one bifurcations occur in its unfolding.

Specifically, at a cusp-cusp bifurcation there is a quadratic tangency of an invariant curve W with the singular locus J_0 exactly at the pre-cusp point C_0. This situation corresponds to a cusp of $f(W)$ exactly at the cusp C_1 on J_1, hence, the name of this bifurcation. The situation is of codimension two because one parameter is needed to ensure a tangency of W with J_0, while another parameter must be adjusted to ensure that this tangency occurs at C_0. Recall that the existence of an isolated cusp point on J_1 is a generic property, that is, a cusp point is stable under small parameter variations. Therefore, we assume that the unfolding parameters of the cusp-cusp bifurcation do not lead to bifurcations of the cusp point (such as the disapearance of the cusp point in a swallowtail bifurcation).

We derive a normal form of the cusp-cusp bifurcation by considering the interaction of a parabola (representing W locally) under the action of a normal-form map given by projections via the graph of the function f in $\mathbb{R}^4$ near a generic cusp point. This surface can best be viewed in projection onto $\mathbb{R}^3$, where it takes the form of a generic two-dimensional surface with a cusp as known from singularity theory [4]. In this setup both the cusp point C_1 and the pre-cusp point C_0 are at the origin and the curve J_0 is a fixed parabola with C_0 as its maximum. The unfolding or primary parameters in the normal form are the vertical and horizontal positions of the maximum or minimum of the parabola representing W, while its 'steepness' (relative to the curve J_0) plays the role of a higher-order or secondary parameter in the normal form. Depending on its value we distinguish eight different kinds of cusp-cusp bifurcations with associated two-parameter unfoldings. All unfoldings (cases I to VIII) are presented as two-parameter diagrams with associated representative phase portraits, that is, configurations of W near J_0 and $f(W)$ near J_1. We also show that the phase portraits found in [10] are organized by a cusp-cusp bifurcation of type VII.

Singularity theory is the main tool in our analysis of the cusp-cusp bifurcation. It has proven its use in the bifurcation analysis of invertible maps and vector fields, where classic singularities occur in the product of phase space and parameter space; see [12] and also [5] for a recent example. The question in the present setting is how a noninvertible planar map is folding the phase plane over itself. In other words, one needs to study projections via a surface, namely the smooth image of the domain, in a higher-dimensional space. This point of view has been adopted before, for example, in [32]. The action of a noninvertible planar map near any of the fold curves that make up J_1 can be understood by considering projections via a surface in $\mathbb{R}^3$ with a generic fold line [14, 15]. Similarly, the action of a noninvertible planar map near a cusp in terms of projections via a cusp surface has been discussed in [24]. Note, however, that the singularity theory point of view has mostly been used for illustration of the action of the map. Its use for a systematic bifurcation analysis of noninvertible maps is new. In [7] projections via a folded surface were used to identify two types of codimension-one tangency bifurcations of a stable set with J_1 that are responsible for any rearrangements of the basins of attractions of a noninvertible map. The study presented here is very much in the same spirit. Note that near folds and cusps, the

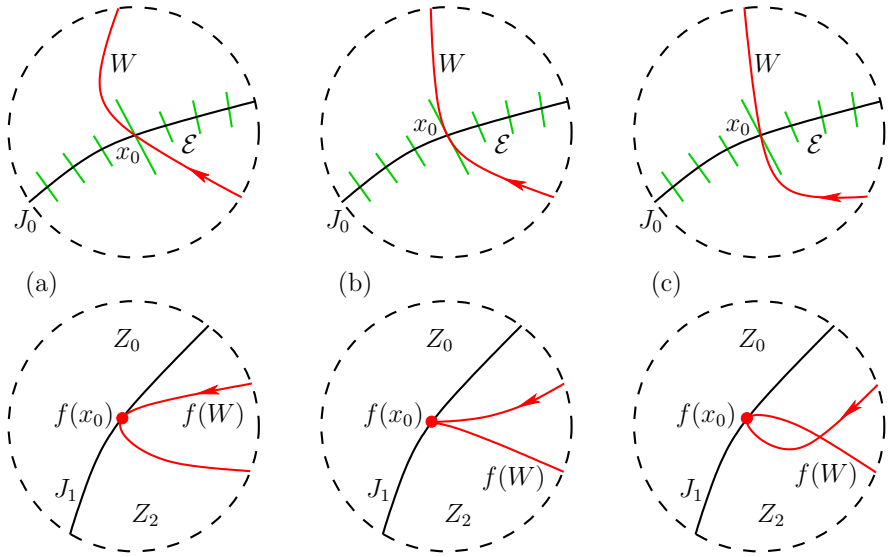

FIG. 2.1. Sketches of the situation before (a), at (b), and after (c) a codimension-one loop creation, where the invariant curve W becomes tangent at x_0 to the line field $\mathcal{E}$ (green curves) (top row), which results in the creation of a little loop of $f(W)$ (bottom row).

situations considered here, the surface via which one projects can be embedded in $\mathbb{R}^3$, rather than in $\mathbb{R}^4$, which greatly helps with visualising the local map.

Another important ingredient of our study is a suitable notion of equivalence that allows one to define codimension-one bifurcations in this context. We consider here topological equivalence as given by the position of the oriented invariant curve relative to J_1; see Definition 3.4.

The paper is organized as follows. In Sec. 2 we discuss some mathematical background, including the normal form of a smooth map near a cusp point. In Sec. 3 we introduce the normal-form setting of the cusp-cusp bifurcation, as well as our notion of topological equivalence of invariant curves relative to J_1. In Sec. 4 we discuss the codimension-one bifurcations that occur near a cusp-cusp bifurcation, and in Sec. 5 we present all cases of two-parameter unfoldings. The adaptive control system from [10] is studied in Sec. 6 to show how our results manifest themselves in practice. We conclude in Sec. 7, where we also point out directions for future research.

2. Mathematical setting and cusp normal-form map. In order to understand the folding properties of f we consider the line field $\mathcal{E}$ accociated with J_0, defined by

$$\mathcal{E} = \{l(e_0(x), x) \mid x \in J_0\}, \tag{2.1}$$

where $l(v, p)$ is the line through the point p given by the vector v, and $e_0(x)$ is the eigenvector of the eigenvalue 0 of $Df(x)$. As stated in Proposition 1.1, every line $\mathcal{E}_x := l(e_0(x), x)$ is transverse to J_0 at generic $x \in J_0$.

Now consider a curve W crossing J_0 transversely. Its image $f(W)$ under f is generically tangent to J_1. This tangency at J_1 is structurally stable, because it corresponds to the projection of a curve that crosses a fold [4]. The exceptional case is

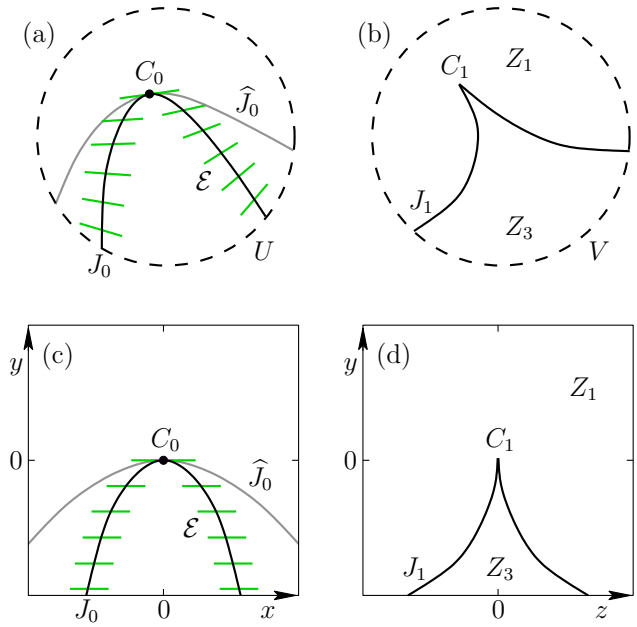

Fig. 2.2. The line field $\mathcal{E}$ at J_0 and its image $f(\mathcal{E})$ at J_1 (green curves) in neighborhoods U of the pre-cusp point C_0 (a), and V of the cusp point C_1 (b). Panels (c) and (d) show the situation for the normal-form map (2.2), where J_0 and $\widehat{J}_0$ are parabolas and the leaves of $\mathcal{E}$ and $f(\mathcal{E})$ are given by $\{y = const.\}$.

given by the line field $\mathcal{E}$. Any curve W that crosses J_0 tangent to $\mathcal{E}$ is mapped such that $f(W)$ has a cusp point on J_1. The directional derivative of $f(W)$ at the cusp point is determined by the curvature of W.

To illustrate the concept we present in Fig. 2.1 the unfolding of the loop creation bifurcation; the top row shows a neighborhood of a transverse intersection point x_0 of a forward invariant curve W with J_0, and the bottom row a neighborhood around $f(x_0)$ on J_1. Note that both W and $f(W)$ have a direction, indicated by arrows, which need to be specified to understand the action of the map. Generically, the tangent $dW(x_0)$ of W at x_0 is transverse to the line $\mathcal{E}_{x_0}$, which means that $f(W)$ has a quadratic tangency with J_1; see Fig. 2.1(a) and (c). However, when $l(dW(x_0), x_0) = \mathcal{E}_{x_0}$ then $f(W)$ has a cusp at $f(x_0) \in J_1$; see Fig. 2.1(b). Geometrically, $f(W)$ passes over the fold curve exactly perpendicularly. In the unfolding of this codimension-one situation a small loop of $f(W)$ is created (or destroyed) near $f(x_0)$, which explains the name of this bifurcation.

2.1. Characterization of a cusp of J_1. We now consider the basic setting of this paper, namely, an isolated generic cusp point C_1 on J_1 and, thus, an isolated pre-cusp point C_0 on J_0. The situation is sketched in Fig. 2.2(a) and (b) in neighborhoods U and V around C_0 and C_1, respectively. Note that J_1 has a second pre-image, denoted $\widehat{J}_0 \subset f^{-1}(J_1)$, in the neighborhood U, which is tangent to J_0 at the pre-cusp point C_0. The three regions below J_0 and in between $\widehat{J}_0$ and J_0 get mapped to the single region with three pre-images, which is the region under the cusp point C_1 and bounded by J_1. This situation is referred to in the literature as a map of type $(Z_1\text{–}Z_3\text{–}Z_1)$. We remark that any map of type $(Z_k\text{–}Z_{k+2}\text{–}Z_k)$ for $k \geq 1$ has the same

properties locally near the cusp point, but with $(k-1)$ additional sheets of inverses that play no role in the local unfolding.

Figure 2.2 also shows the line field $\mathcal{E}$ near J_0. Notice that the line $\mathcal{E}_{C_0}$ is not transverse to J_0. Therefore, the defining property of the cusp-cusp bifurcation, namely a quadratic tangency of an invariant curve W with J_0 at C_0, can be interpreted as defining a degenerate loop bifurcation.

2.2. Cusp normal-form map. As is known from singularity theory [4], a generic smooth planar map with a cusp point can locally near the pre-cusp point be brought to the normal form

$$(x, y) \mapsto (u, v) = (axy - bx^3, y)$$

by a smooth change of variables, for any positive nonzero constants a and b. We make a convenient choice, namely we consider the normal-form map defined as

$$F : \begin{pmatrix} x \\ y \end{pmatrix} \mapsto \begin{pmatrix} z \\ y \end{pmatrix} = \begin{pmatrix} -x^3 - 3xy \\ y \end{pmatrix}. \tag{2.2}$$

The (x, y)-plane corresponds to a local neighborhood of C_0 and the (z, y)-plane to a local neighborhood of C_1. Both C_0 and C_1 are located at the origin. The exact form of (2.2) was chosen such that the Jacobian

$$DF \begin{pmatrix} x \\ y \end{pmatrix} = \begin{bmatrix} -3x^2 - 3y & -3x \\ 0 & 1 \end{bmatrix}$$

is singular along the particularly simple critical curve

$$J_0 := \{y = -x^2\}. \tag{2.3}$$

The image of the parabola J_0 is the standard cusp

$$J_1 := \{z = \pm 2(\sqrt{-y})^3 \mid y \leq 0\}. \tag{2.4}$$

A straightforward calculation shows that it has the second pre-image

$$\widehat{J}_0 := \{y = -\tfrac{1}{4}x^2\}. \tag{2.5}$$

The line field $\mathcal{E}$ does not depend on x and consists simply of the lines $\{y = 0\}$.

The situation for the normal-form map F is shown in Fig. 2.2(c) and (d) in neighborhoods around C_0 and C_1, respectively. Note that the coordinate change that transforms a generic map f near a cusp point into its normal form F deforms the curves J_0 and $\widehat{J}_0$ to parabolas and the curve J_1 to a standard cusp. Furthermore, it 'stretches out' the line field $\mathcal{E}$ to horizontal lines.

Figure 2.3 shows how the action of the map F can be interpreted geometrically as a projection via the cusp surface $\mathcal{S}$ in (x, y, z)-space given by $-x^3 - 3xy - z = 0$. Note that $\mathcal{S}$ is a graph over the (x, y)-plane, but not over the (z, y)-plane. Any point (x_0, y_0) in the (x, y)-plane corresponds to a unique point on $\mathcal{S}$ under projection in the z-direction. It is then mapped to the unique point $F(x_0, y_0)$ under projection in the x-direction. Conversely, a point (z_0, y_0) in the (z, y)-plane lifts to a single point on $\mathcal{S}$ in the region of unique pre-images, to two points on $\mathcal{S}$ if $(z_0, y_0) \in J_1$, and to three points on $\mathcal{S}$ in the region of three pre-images. Notice also the (projection of) the curves J_0 and $\widehat{J}_0$ on $\mathcal{S}$.

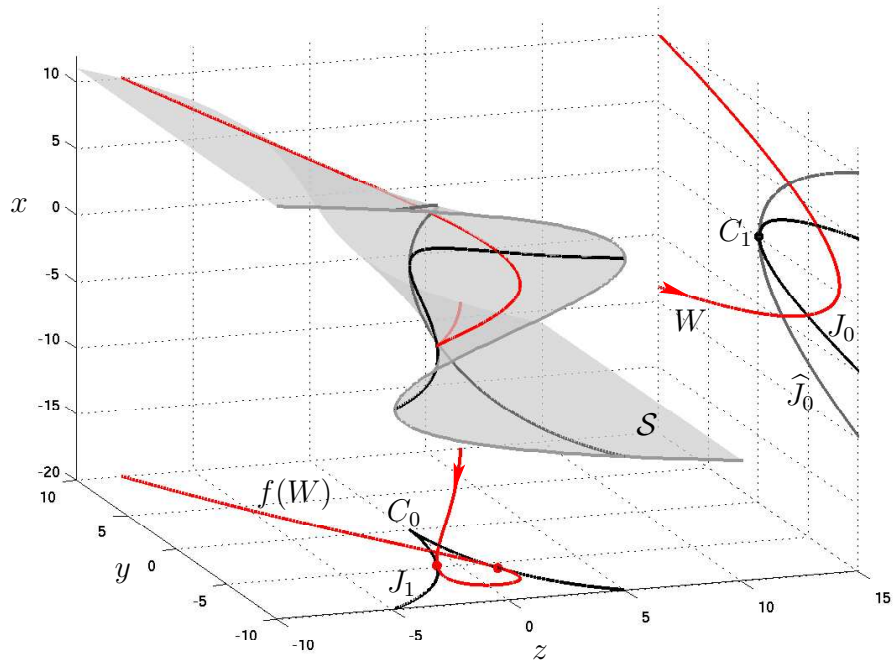

FIG. 2.3. Visualization in (x, y, z)-space of how the normal-form map (2.2) can be interpreted as a projection via the cusp surface $\mathcal{S}$. The curve W in the (x, y)-plane is mapped to the curve $F(W)$ in the (z, y)-plane; the example is phase portrait 31 of Fig. 5.2.

Figure 2.3 also shows how a parabola in the (x, y)-plane 'around' the pre-cusp point maps under F. The result is a curve in the (z, y)-plane with a self-intersection and two tangencies with J_1, one at either side of the cusp point. This can be understood by considering the projection of the parabola onto the cusp surface $\mathcal{S}$, and then down to the (z, y)-plane.

3. Normal-form setting of the cusp-cusp bifurcation. At the cusp-cusp bifurcation there is a tangency of an invariant curve W with the curve J_0 at a pre-cusp point C_0. As a consequence, $f(W)$ has a cusp exactly at the cusp point C_1 on J_1. This codimension-two bifurcation can be classified as a global bifurcation, because it involves an invariant curve. Nevertheless, we can consider a normal-form setting in the small neighborhoods U and V of C_0 and C_1, respectively, by replacing f near C_0 with the normal-form map F as given by (2.2). Then the curves J_0 and $\widehat{J}_0$ are the parabolas given by (2.3) and (2.5) and the points C_0 and C_1 are at the origin of the (x, y)- and (z, y)-planes, respectively. Furthermore, the tangency of W with J_0 at C_0 is generically quadratic. As a consequence, in any unfolding the intersections of W with J_0 and $\widehat{J}_0$ in a sufficiently small neighborhood U are determined entirely by the quadratic nature of the curve W. Therefore, from now on we consider the *quadratic normal form for* W in the (x, y)-plane given by

$$W := \{y = \gamma(x - a)^2 + b\}. \tag{3.1}$$

Here the parameters $a, b \in \mathbb{R}$ are the primary unfolding parameters and $\gamma \in \mathbb{R}$ is a higher-order or secondary parameter that determines the 'steepness' of W relative to

the fixed parabolas J_0 and $\widehat{J}_0$. The invariant curve in the neighborhood V of C_1 is simply given by $F(W)$. Note that the maximum (for $\gamma < 0$) or minimum (for $\gamma > 0$) of W lies at $(x, y) = (a, b)$; the cusp-cusp bifurcation occurs for $a = b = 0$.

The normal-form setting of the cusp-cusp bifurcation is now given as the study of all possible different configurations of $F(W)$ relative to J_1 and C_1 as a function of the unfolding parameters a and b, and for fixed generic values of the higher-order term γ. These different configurations correspond one-to-one to different types of intersections of W with J_0 and $\widehat{J}_0$; see already Definition 3.4.

Throughout this paper we use the convention that the orientation of W is from left to right, that is, in the direction of increasing x. The orientation of $F(W)$ is induced by this convention. Notice that the map F reverses the orientation of the invariant curve in Fig. 2.3, which is illustrated by the arrows of W and $F(W)$. We have the following general result.

PROPOSITION 3.1 (Orientation of $F(W)$). *For any a and b the image $F(W)$ of an (oriented) parabola W of the form (3.1) is oriented from left to right if $\gamma < -\frac{1}{3}$ and from right to left for $\gamma > -\frac{1}{3}$; see also Fig. 3.1(c)–(e).*

Proof. The curve

$$R_0 := \{y = -\frac{1}{3}x^2\} \tag{3.2}$$

in the (x, y)-plane is mapped under the normal-form map F in a two-to-one fashion to the line segment $\{z = 0 \text{ and } y \leq 0\}$ in the (z, y)-plane. The region above R_0 is mapped to the (z, y)-plane in an orientation reverserving way, that is, positive x are mapped to negative z. By contrast, the region below R_0 is mapped to the (z, y)-plane in an orientation preserving way. The result follows, since the segments for sufficiently large $\mid x \mid$ of a parabola of the form (3.1) both lie in either one of the two regions. □

3.1. The cusp-cusp singularity. The nature of the cusp-cusp singularity for $(a, b) = (0, 0)$ depends on the higher-order term γ of (3.1). For $(a, b) = (0, 0)$ and for generic γ the cusp point C_1 is the only intersection point of $F(W)$ and J_1. The exception is that $F(W) \equiv J_1$, which happens when either $W = J_0$ or $W = \widehat{J}_0$. We further distinguish different cases of the cusp-cusp singularity depending on

- the orientation of $F(W)$,
- whether the curve $F(W)$ is below or above J_1, and
- whether or not the cusp of $F(W)$ at C_1 points upwards or downwards.

PROPOSITION 3.2 (Cusp-cusp singularity). *There are five intervals on the γ-line of generic cusp-cusp singularities for $(a, b) = (0, 0)$ in (3.1). The boundary points between these intervals are given by $\gamma = -1$, $\gamma = -\frac{1}{3}$, $\gamma = -\frac{1}{4}$, and $\gamma = 0$.*

Proof. According to Proposition 3.1 the orientation of $F(W)$ changes when W crosses R_0, which gives rise to the boundary point $\gamma = -\frac{1}{3}$. Furthermore, for $W = J_0$ or $W = \widehat{J}_0$ we have that $F(W) = J_1$, which gives rise to the boundary points $\gamma = -1$ and $\gamma = -\frac{1}{4}$, respectively. For W above $\widehat{J}_0$, that is, for $\gamma > -\frac{1}{4}$ the curve $F(W)$ lies above J_1. It follows immediately from (2.2) that the cusp of $F(W)$ is approached from the direction of negatitive y for any $\gamma < 0$ and from the direction of positive y for $\gamma > 0$. The situation for $\gamma = 0$ is degenerate in that $F(W)$ does not have a cusp at all. □

Proposition 3.2 is illustrated in Fig. 3.1, where panels (a), (c), (e), (g) and (i) show the generic cases for $(a, b) = (0, 0)$. Note that panels (a) and (c) do not differ either

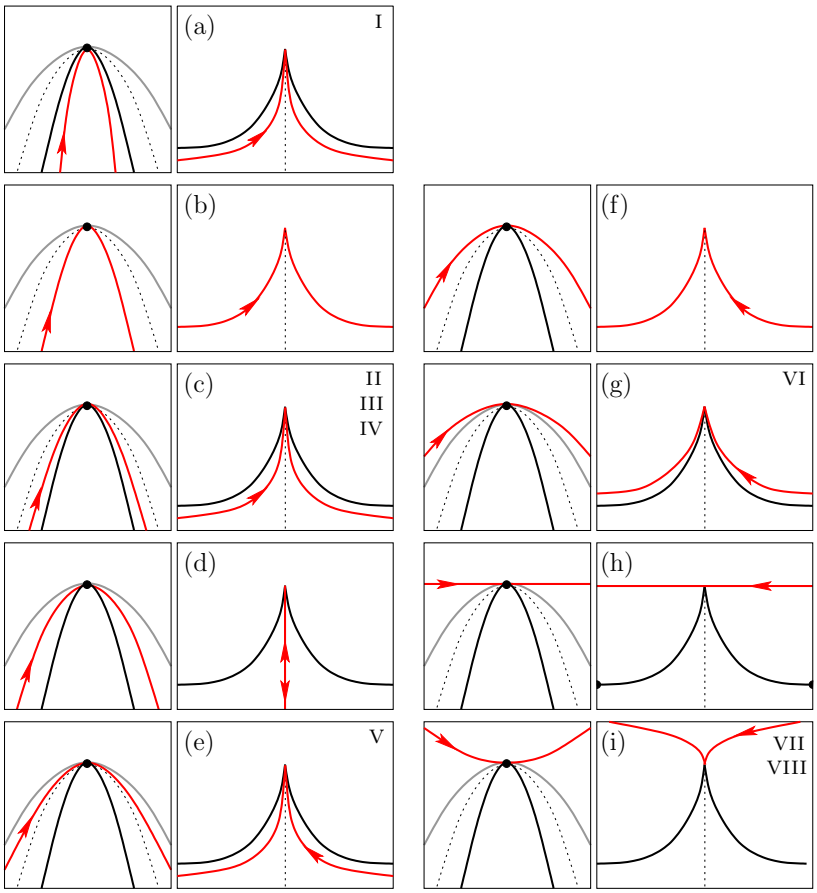

Fig. 3.1. Sketches of all generic and non-generic cases of the cusp-cusp singularity; see Proposition 3.2. The left-hand panels show W (red curve) near the pre-cusp point C_0, and the right-hand panels shown $f(W)$ (red curve) in relation to J_1. The curves J_0 and J_1 are black, $\widehat{J}_0$ is grey, and R_0 is dashed and double-covers the dashed straight line; the arrows show the direction of parametrization by x. Shown are $\gamma < -1$ (a), $\gamma = -1$ (b), $-1 < \gamma < -\frac{1}{3}$ (c), $\gamma = -\frac{1}{3}$ (d), $-\frac{1}{3} < \gamma < -\frac{1}{4}$ (e), $\gamma = -\frac{1}{4}$ (f), $-\frac{1}{4} < \gamma < 0$ (g), $\gamma = 0$ (h), and $0 < \gamma$ (i). For the generic cases in panels (a), (c), (e), g) and (i) the associated two-parameter unfoldings of Fig. 5.1 are indicated.

in position or orientation in the (z, y)-plane. The difference is that the corresponding curve lies on different sheets of the cusp surface $\mathcal{S}$ (see also Fig. 2.3) and, as we will see in Sec. 5, this leads to different two-parameter unfoldings. Figure 3.1(b), (d), (f) and (h) show the degenerate situations at the boundary points, namely, the situations when $W = J_0$, $W = R_0$, $W = \widehat{J}_0$ and $W \equiv 0$, respectively.

3.2. Topological equivalence. In order to speak of typical or generic situations and their bifurcations we now define a general notion of topological equivalence that formalizes the informal concept of 'different configurations of an invariant curve relative to J_1 and C_1'. For notational convenience we give the definiton in the context of the normal-form setting. However, it can be extended in a straightforward manner to define the topological equivalence of two general invariant curves relative to J_1 in two respective neighborhoods of a cusp point and the corresponding pre-cusp point.

DEFINITION 3.3 (Generic event). *Consider the image $F(W)$ of the (oriented) parabola W given by (3.1) under the normal-form map F. A* generic event *is either*

- *a quadratic tangency of $F(W)$ with J_1 at a generic point on J_1 (in a neighborhood of which J_1 is locally a smooth curve), or*
- *a transverse intersection of $F(W)$ and J_1 at a generic point on J_1.*
- *an isolated self-intersection of $F(W)$,*

In the fist two cases we say that two such generic events are of the same type *if the respective tangency or intersection points*

1. *both lie on the same side of the cusp point C_1 on J_1, that is, both occur for $z < 0$ or both for $z > 0$, and*
2. *they are passed by $F(W)$ (locally) in the same direction, that is, both towards increasing z or both towards decreasing z.*

We are now able to define topological equivalence between generic situations, based on the notion of generic events. Note that a cusp on W is not generic.

DEFINITION 3.4 (Topological equivalence of an invariant curve relatve to J_1). *Consider two images $F(W)$ and $F(\widetilde{W})$ of two (oriented) parabolas W and $\widetilde{W}$ given by (3.1) under the normal-form map F. We say that the curves $F(W)$ and $F(\widetilde{W})$ are topologically equivalent with respect to J_1 if they*

1. *have the same induced orientation, and*
2. *both encounter the same types of generic events in the same order.*

The task for the remainder of this paper is to find all equivalence classes of this notion of topological equivalence. Specifically, we need to find all generic two-parameter unfoldings in the (a, b)-plane for different choices of the higher-order term γ in (3.1). We start with a straightforward result on the possible number of events.

PROPOSITION 3.5 (Number of events). *In the normal-form setting of the cusp-cusp bifurcation, that is, for W given by (3.1) and any a, b and generic γ, that is, for $\gamma \notin \{-1, -\frac{2}{3}, -\frac{1}{2}, -\frac{1}{3}, -\frac{1}{4}, 0, 1\}$, there are at most*

- *two tangencies of $F(W)$ with J_1,*
- *two intersection of $F(W)$ with J_1, and*
- *one self-intersection of $F(W)$.*

Proof. The curves W, J_0 and $\widehat{J}_0$ are parabolas and graphs over the x-axis. Therefore, for any a, b and γ, W can have at most two intersections with J_0 or $\widehat{J}_0$, which limits the number of tangencies and intersections of $F(W)$ with J_1 to two as well.

Any self-intersection of $F(W)$ must lie in the region under $\widehat{J}_0$, that is, in the z-interval between the two (if they exist) unique folds of $F(W)$ with respect to z. Furthermore, a self-intersection is due to a pair of points on W with the same y-value. According to (3.1) and (2.2) the curve $F(W)$ covers its y-range in a two-to-one fashion with a single maximum or a single minimum (depending on the sign of γ). Since $F(W)$ has either zero or two folds with respect to z, there can be at most one such pair of points with the same y-value, namely, exactly when the single maximum/minimum of $F(W)$ lies in between the two fold points. □

4. Codimension-one bifurcations. Definition 3.4 gives rise to codimension-one bifurcations that correspond to a transition between equivalence classes of topological equivalence of the curve $F(W)$. There are five basic codimension-one bifurcations where the change is local, that is, it occurs in a small neighborhood of the bifurcation point. Furthermore, we find bifurcations at infinity and a transition due to the degeneracy of the parametrization (3.1).

4.1. The basic codimension-one bifurcations. A great advantage of the normal-form setting is that it is possible to compute the loci of all these bifurcations explicitly.

Proposition 4.1 (Basic codimension-one bifurcations). *In the normal-form setting of the cusp-cusp bifurcation there are exactly five codimension-one bifurcations for $(a,b) \neq (0,0)$ in (3.1) that correspond to a local change of events as defined in Definition 3.4. They are illustrated in Figs. 4.1 and 4.2.*

1. *The* cusp transition, *denoted by C, where the curve W passes through J_0 at the pre-cusp point C_0, which means that $F(W)$ passes exactly through the cusp point C_1 on J_1; see Fig. 4.1(a). The locus of this bifurcation in the (a,b)-plane is the parabola*

$$b = c_C(\gamma)\, a^2 = -\gamma\, a^2. \tag{4.1}$$

2. *The* loop-creation bifurcation, *denoted by L, where W crosses J_0 tangent to the (horizontal) line field $\mathcal{E}$; see Fig. 4.1(b). The locus of this bifurcation in the (a,b)-plane is the parabola*

$$b = c_L(\gamma)\, a^2 = -a^2. \tag{4.2}$$

3. *The* intersection-at-tangency bifurcation, *denoted by I, where $F(W)$ self-intersects at a tangency point with J_1; see Fig. 4.1(c). The locus of this bifurcation in the (a,b)-plane is the parabola*

$$b = c_I(\gamma)\, a^2 = -(9\gamma + 4)\, a^2. \tag{4.3}$$

4. *The* tangency-creation bifurcation, *denoted by T, where W is tangent to J_0; see Fig. 4.2(a). The locus of this bifurcation in the (a,b)-plane is the parabola*

$$b = c_T(\gamma)\, a^2 = -\frac{\gamma}{1+\gamma}\, a^2. \tag{4.4}$$

5. *The* enter-exit bifurcation, *denoted by E, where W is tangent to $\widehat{J}_0$; see Fig. 4.2(b). The locus of this bifurcation in the (a,b)-plane is the parabola*

$$b = c_E(\gamma)\, a^2 = -\frac{\gamma}{1+4\gamma}\, a^2. \tag{4.5}$$

Proof. Each of these bifurcations is defined by a codimension-one condition on the parabola W as given by (3.1), so that their loci can be computed explicitly.
1. By definition of the cusp bifurcation, W passes through the pre-cusp point C_0 at $(x,y) = (0,0)$. Substitution into (3.1) gives the locus.
2. Since the line field $\mathcal{E}$ of the normal-form map F consists of horizontal lines, a loop bifurcation occurs when the extremum at $(x,y) = (a,b)$ of W lies on J_0. Substitution into (3.1) gives the locus.
3. A transversal crossing of W and J_0, say, at (x_0, y_0), corresponds to a tangency of $F(W)$ with J_1. Hence, an intersection-at-tangency bifurcation occurs when W intersects $\widehat{J}_0$ at the same y-value, that is at some point (x_1, y_0). From (2.3) and (2.5) we conclude that then $x_1 = -2x_0$ and we can determine x_0 from

$$\gamma(x_0 - a)^2 + b = \gamma(-2x_0 - a)^2 + b.$$

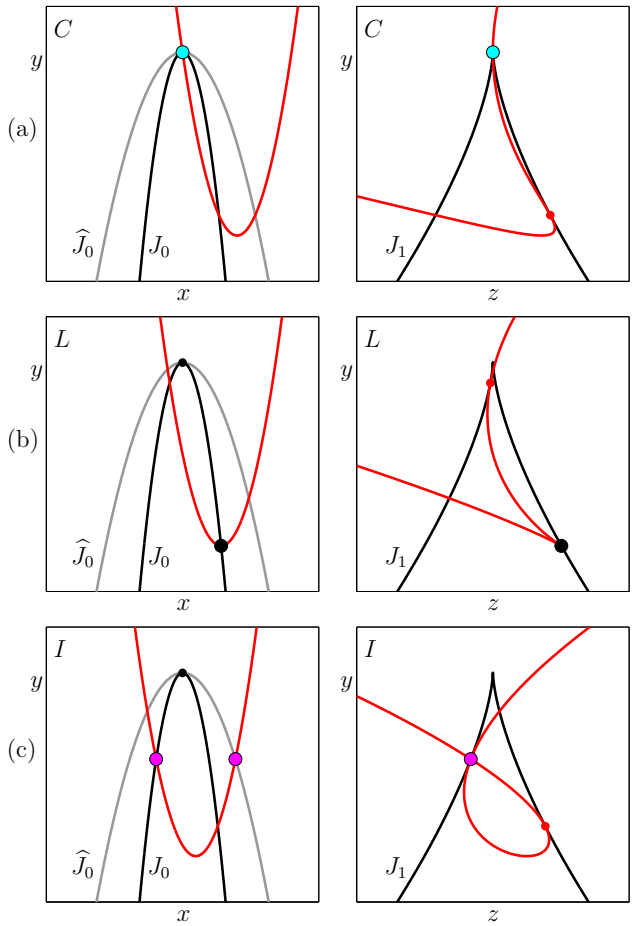

FIG. 4.1. Arrangement of W and $F(W)$ at the cusp-transition bifurcation C (a), the loop-creation L (b), and the intersection-at-tangency bifurcation I (c).

The assumption that the bifurcation does not occur at the origin implies that $x_0 = -2a$. Hence, in order for (x_0, y_0) to lie on J_0, a and b should be such that

$$y_0 = \gamma(x_0 - a)^2 + b = -x_0^2 \Leftrightarrow y_0 = 9\gamma a^2 + b = -4a^2,$$

which gives the locus.

4. At the tangency-creation bifurcation W is tangent to J_0 at, say, $(x_t, y_t) \in J_0 \cap W$. Since the slopes of W and J_0 at (x_t, y_t) must be equal we conclude from (2.3) that

$$\left\{ \begin{array}{rcrcl} y_t & = & \gamma(x_t - a)^2 + b & = & -x_t^2, \\ & & 2\gamma(x_t - a) & = & -2x_t, \end{array} \right.$$

$$\Leftrightarrow \left\{ \begin{array}{rcrcl} y_t & = & \gamma\frac{a^2}{(1+\gamma)^2} + b & = & -\frac{a^2\gamma^2}{(1+\gamma)^2}, \\ x_t & = & \frac{a\gamma}{1+\gamma}, & & \end{array} \right.$$

and this gives the locus.

5. The locus of tangency of W with $\widehat{J}_0$ can be derived exactly as for the tangency with J_0, by using (2.5) instead of (2.3).

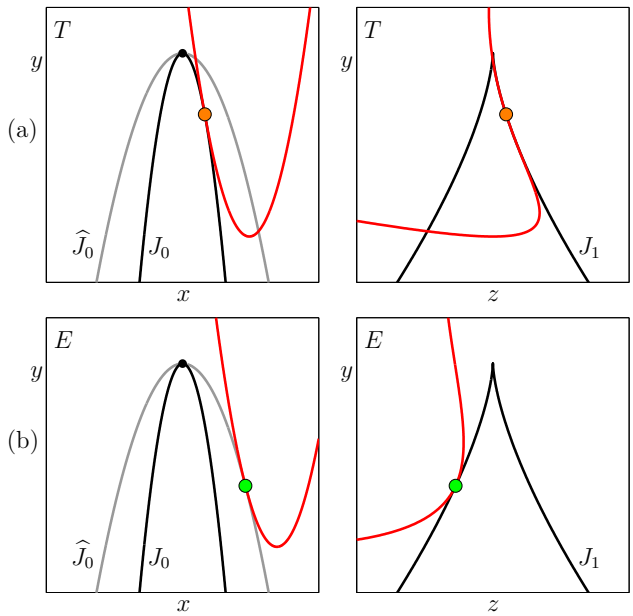

Fig. 4.2. Arrangement of W and $F(W)$ at the tangency creation T (a), and the enter-exit bifurcation E (b).

Finally, there are only these five codimension-one bifurcations because, generically in the normal form setting, W can only either intersect J_0 and $\widehat{J}_0$ transversly, or have a quadratic tangency with J_0 or $\widehat{J}_0$. In particular, higher-codimension singularities, for example, cubic tangencies, are not possible in the normal-form setting. □

Indeed the codimension-one bifurcations of Proposition 4.1 give rise to topologically different configurations of $F(W)$ and J_1. The first three bifurcations correspond to transverse intersection of W and J_0. At the cusp transition bifurcation, a tangency point of $F(W)$ with J_1 moves from the left to the right of the cusp point C_1. At the loop-creation bifurcation a small loop, that is, a self-intersection, is created; see also Fig. 2.1. At the intersection-at-tangency bifurcation there is an exchange of the order along $F(W)$ between a self-intersection of $F(W)$ and a (generic) tangency between $F(W)$ and J_1. The other two bifurcations correspond to codimension-one tangencies of W with J_0 and $\widehat{J}_0$. At a tangency creation two transverse intersections of W and J_0 and, hence, two (generic) tangencies between $F(W)$ and J_1, are created. At the enter-exit bifurction two transverse intersections of $F(W)$ and J_1 are created.

4.2. Representation on the Poincaré disk and bifurcations at infinity. Events as defined in Definition 3.4 can move outside a fixed neighborhood of interest, which changes the topological type of $F(W)$ inside this neighborhood by changing the number of events that one encounters. In order to represent the entire topological structure in a compact region, we now introduce the representation of the (x, y)- and (z, y)-planes on the Poincaré disk. The representation on the Poincaré disk is quite popular in bifurcation theory, because any dynamically relevant object can be kept track of even if they bifurcate at (the circle representing) infinity; see, for example, [20].

The Poincaré disk is obtained by 'closing off' the plane $\mathbb{R}^2$ with a circle that

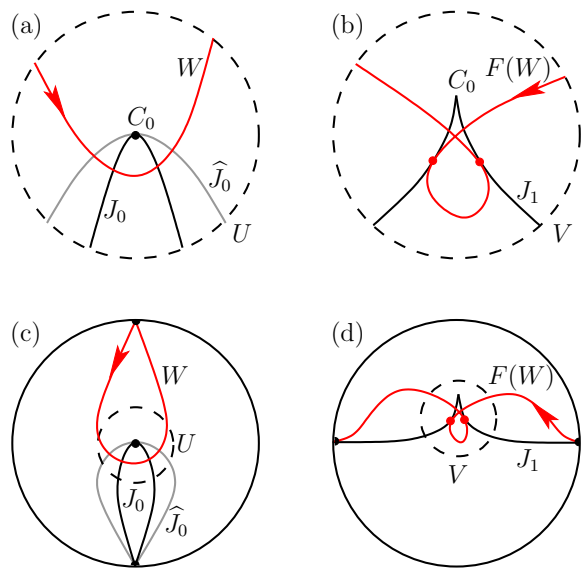

FIG. 4.3. The local interaction of W with J_1 and $\widehat{J}_0$ in a neighborhood U (a) corresponds to the the local interaction of $F(W)$ with J_1 in a neighborhood V (b). Panels (c) and (d) show the same situation sketched on the Poincaré disk. The example is phase portrait 31; compare with Fig. 2.3.

represents the asymptotic directions of curves at infinity. The phase plane is then represented on the unit disk, where points $e^{i\phi}$ on the unit circle correspond to the directional limits ϕ. In the present situation we are concerned with the curve W relative to J_0 and $\widehat{J}_0$, all of which are parabolas and graphs over the horizontal x-axis. Hence, the directional limits of J_0 and $\widehat{J}_0$ for $x \to \pm\infty$ are $-\pi/2$, so that these curves start and end on the Poincaré disk at the point $-i = e^{-\pi i/2}$. Similarly, the curve W starts and ends at $-i$ for $\gamma < 0$ and at i for $\gamma > 0$. The curve J_1, on the other hand, has the directional limits 0 and π, and the same is true for the image of any parabola as given by (3.1) for any values of a, b and γ. Therefore, J_1 and $F(W)$ have the limits -1 and $+1$ on the Poincaré disk. The situation is illustrated in Fig. 4.3 for the phase portrait from Fig. 2.3, that is, $\gamma > 0$. Panel (a) of Fig. 4.3 shows the local picture near J_0 and panel (c) the corresponding picture on the Poincaré disk. The respective images are shown in panels (c) and (d). This is illustrated in Fig. 4.3(d) for the local picture in panel (b).

We have the following result concerning bifurcations of phase portraits on the Poincaré disk.

PROPOSITION 4.2 (Bifurcations at infinity). *In the normal-form setting of the cusp-cusp bifurcation with W given by (3.1) there are three bifurcations at infinity on the Poincaré disk that change the equivalence class of topological equivalence of Definition 3.4.*

1. *The* tangency at infinity, *where a generic tangency of $F(W)$ with J_1 moves via infinity from one side of the cusp point C_1 to the other. The locus of this bifurcation is given by $\gamma = -1$, which is the vertical asymptote of the coefficient of the tangency creation $c_T(\gamma) = -\frac{\gamma}{1+\gamma}$; see (4.4) and, for example, the transition between phase portraits 2 and 9 in Fig. 5.2.*

2. *The* intersection at infinity*, where a transverse intersection of $F(W)$ and J_1 moves via infinity from one side of the cusp point C_1 to the other. The locus of this bifurcation is given by $\gamma = -\frac{1}{4}$, which is the vertical asymptote of the coefficient of the enter-exit bifurcation $c_E(\gamma) = -\frac{\gamma}{1+4\gamma}$; see (4.5) and, for example, the transition between phase portraits 15 and 22 in Fig. 5.2.*
3. *The* self-intersection at infinity*, where a self-intersection of $F(W)$ bifurcates at the boundary of the Poincaré disk. This happens by a swap between the begin and end points of $F(W)$ at ± 1, and this also results in a change of direction of $F(W)$. The locus of this bifurcation is given by $\gamma = -\frac{1}{3}$, which corresponds to the crossing of W and R_0; see (3.2) and, for example, the transition between phase portraits 7 and 15 in Fig. 5.2.*

Proof. The respective topological changes and their loci follow immediately from the fact that the loci of the tangency bifurcation and the enter-exit bifurcation have asymptotes.

For any fixed values of a and b the limits for $x \to \pm\infty$ of the parabola W lie below the curve R_0 if $\gamma < -\frac{1}{3}$, and above the curve R_0 if $\gamma > -\frac{1}{3}$. This means that the directional limits of $F(W)$ change when γ crosses $-\frac{1}{3}$. Effectively, the two ends of $F(W)$ reconnect differently to the points ± 1 on the boundary of the Poincaré disk. Note that for the degenerate case of $\gamma = -\frac{1}{3}$ they both approach the curve $\{z = 0\}$, that is, the point $-i$ on the boundary of the Poincaré disk. One can view this as an 'ambivalent connection' to the points ± 1 via the lower quarters of the circle at infinity. □

4.3. Inversion near the cusp. As we discuss now, there is one more possibility for transitions between equivalence classes of $F(W)$. Recall that according to Proposition 3.2 the passage through the degenerate case $\gamma = 0$ changes the topological type of the central singularity for $(a, b) = (0, 0)$. This also has consequences if $F(W)$ for $(a, b) \neq (0, 0)$.

Proposition 4.3 (Inversion near cusp). *The parabola W given by (3.1) has a maximum for $\gamma < 0$ and a minimum for $\gamma > 0$. As a result, near the cusp point C_1 on J_1 the curve $F(W)$ has a local maximum for $\gamma < 0$ and a local minimum for $\gamma > 0$. We call the transition through the degenerate case $\gamma = 0$ the* inversion near the cusp*, and it results in a topological change of $F(W)$ in the case that this curve interacts with J_1; see, for example, the transition between phase portraits 24 and 29 in Fig. 5.2.*

Note that the inversion near the cusp is not a bifurcation in a classical sense. Rather it is a degeneracy of the parametrization, which changes the direction in which $F(W)$ approaches a neighborhood of the cusp point C_1. This manifests itself quite dramatically as a type of 'inversion' in this neighborhood. There are actually only three different transitions featuring an inversion near the cusp; see already Fig. 5.1 and Fig. 5.2, and compare panels 24 to 29, 25 with 30, and 26 with 31. We refer to the inversion near the cusp loosely as a bifurcation (albeit an unusual one) of codimension-one, because it forms a codimension-one boundary between equivalence classes of $F(W)$ in (a, b, γ)-space.

5. Two-parameter unfoldings in the (a, b)-plane. The five codimension-one bifurcations of Sec. 4.1 are all given by parabolas $b = c_*(\gamma)\, a^2$ through the origin. Hence, the bifurcation diagram in the (a, b)-plane is determined entirely by the ordering of the respective bifurcations, which is given by the sizes of the coefficients $c_*(\gamma)$.

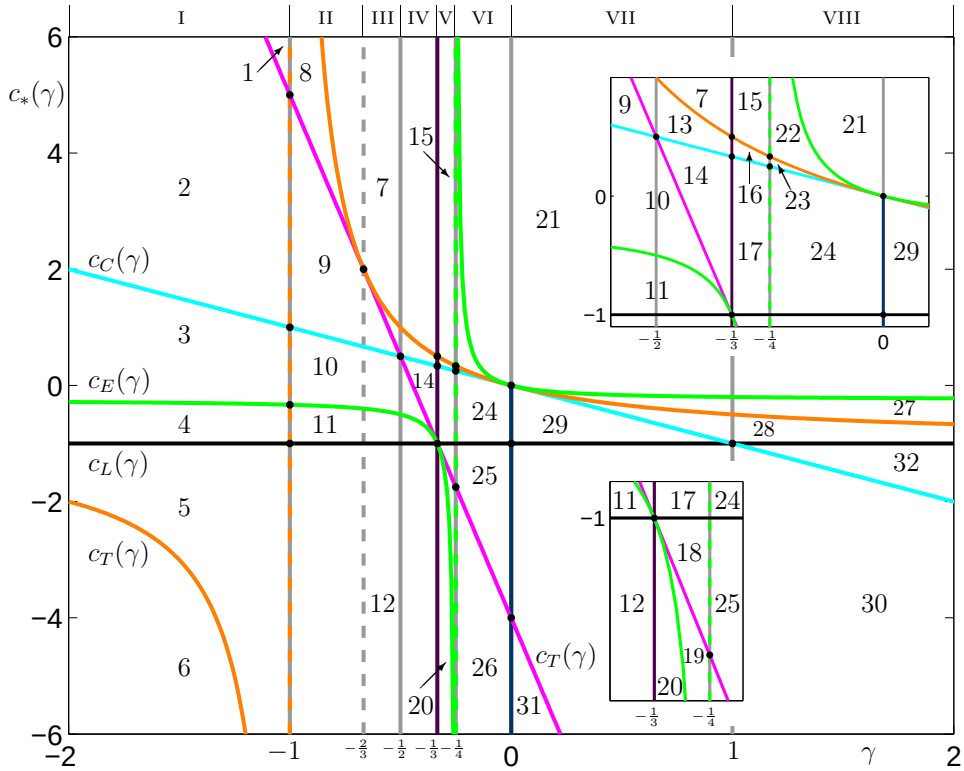

FIG. 5.1. Division of the $(\gamma, c_*(\gamma))$-plane into regions of different phase portraits for $a > 0$, which are shown in Fig. 5.2; see Proposition 5.1. The γ-axis is divided into regions of different two-parameter unfoldings, cases I–VIII, which are shown individually in Figs. 5.3 to 5.10. The colors of the dividing codimension-one bifurcations from Proposition 4.1 are as introduced in Figs. 4.1 and 4.2; the dash-colored vertical curves are the corresponding bifurcations at infinity from Proposition 4.2; the vertical dark blue line is the inversion near the cusp from Proposition 4.3.

In Fig. 5.1 we show all information on the cusp-cusp unfolding in a convenient and very condensed representation by plotting the graphs of the functions $c_*(\gamma)$. This corresponds geometrically to showing how the slices $\{a = \pm 1\}$ in the (a, b)-plane change with γ. The different bifurcations are shown in different colors as introduced in Figs. 4.1 and 4.2. In this representation the other bifurcations in Secs. 4.2 and 4.3 are vertical lines since they do not depend on a and b.

The set of all bifurcation curves divides the $(\gamma, c_*(\gamma))$-plane into 32 regions of topologically equivalent phase portraits; the insets show enlargements of two rather small regions. Representatives of all 32 phase portraits that one finds for $a > 0$ are shown as sketches on the Poincaré disk in Fig. 5.2. Since all bifurcation curves in the (a, b)-plane are parabolas through the origin, the bifurcation diagram is symmetric under the operation $a \mapsto -a$. It follows directly from (2.2) and (3.1) that the corresponding phase portraits for $a < 0$ are obtained by reflecting the curve $F(W)$ on the y-axis on the (z, y)-plane without changing its orientation, so that all events (see Definition 3.3) now occur on the opposite side of C_1 and in the reverse order. We call the thus obtained phase portrait the *conjugate phase portrait* and denote it by a bar across the number. Note that a phase portraits and its conjugate are generally not

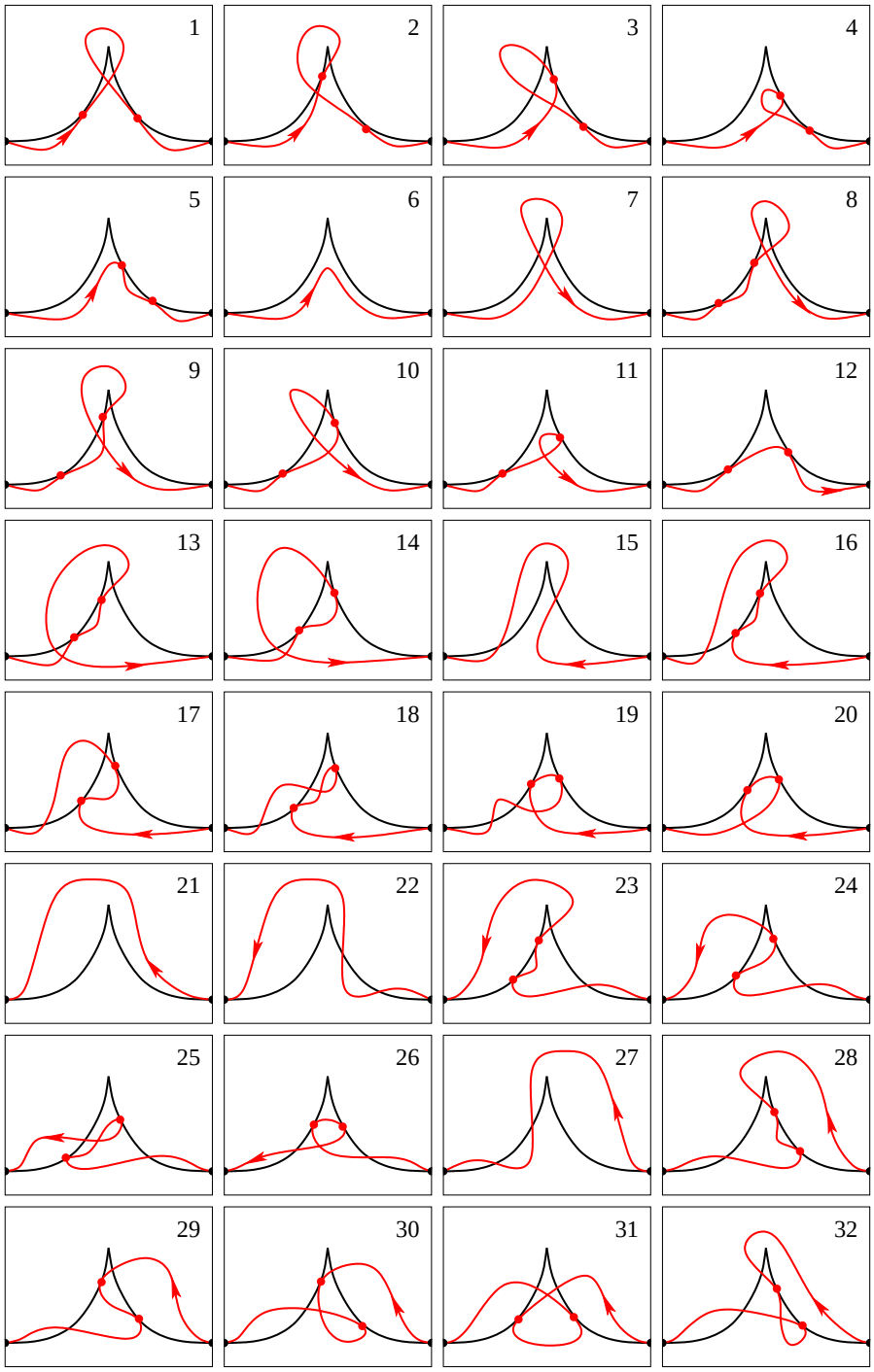

Fig. 5.2. Sketches on the Poincaré disk of all generic phase portraits for $a > 0$ of $F(W)$ (red curve) in relation to J_1 (black curve); the arrows show the direction of parametrization by x. The respective phase portraits for $a < 0$ are obtained by the operation of conjugation.

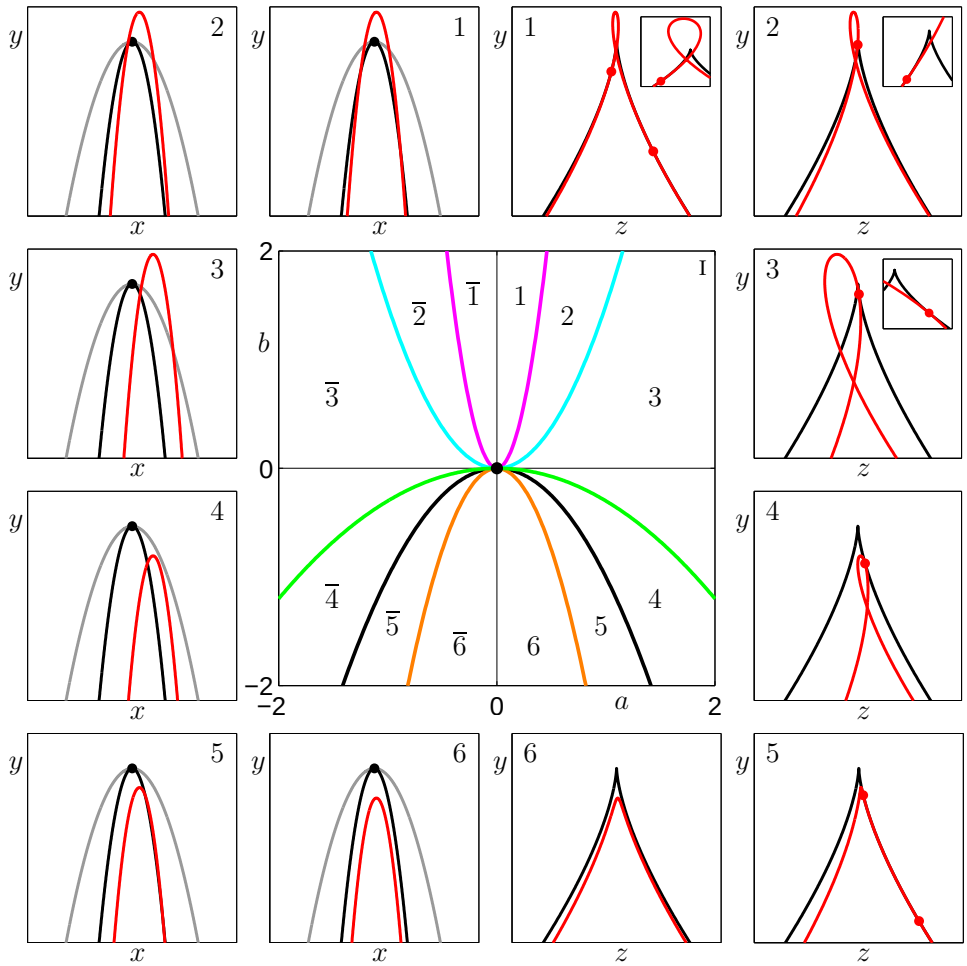

FIG. 5.3. Case I: $-\infty < \gamma < -1$
The two-parameter unfolding in the (a, b)-plane with the bifurcation curves C (blue), L (black), I (purple), T (orange), and E (green); compare with Figs. 4.1 and 4.2. Representative phase portraits near C_0 are presented anti-clockwise from the second image at the top, and near C_1 clockwise from the third image at the top; shown are W and $F(W)$ (red curves), J_0 and J_1 (black curves), and $\widehat{J}_0$ (grey curve). The data is for $\gamma = -1.5$, with phase portraits for $(a, b) = (0.2, 1.7)$, $(a, b) = (0.7, 1.7)$, $(a, b) = (2.0, 1.7)$, $(a, b) = (2.0, -1.7)$, $(a, b) = (0.7, -1.1)$, and $(a, b) = (0.2, -1.7)$, respectively.

topologically equivalent.

The unfoldings represented in Figs. 5.1 and 5.2 were obtained by a combination of analysis and topological arguments — guided by exploration on the computer. We stress again that in the normal-form setting all bifurcation curves can be found analytically. Furthermore, phase portraits can be explored simply by plotting $F(W)$ relative to J_1 for appropriate values of a, b and γ. The overal result can be summarized as follows.

PROPOSITION 5.1 (Two-parameter unfoldings). *There are eight two-parameter unfoldings in the (a, b)-plane, denoted* I–VIII, *as shown in Figs. 5.1. The boundary points between the respective intervals of the γ-line are* -1, $-\frac{2}{3}$, $-\frac{1}{2}$, $-\frac{1}{3}$, $-\frac{1}{4}$, 0, *and*

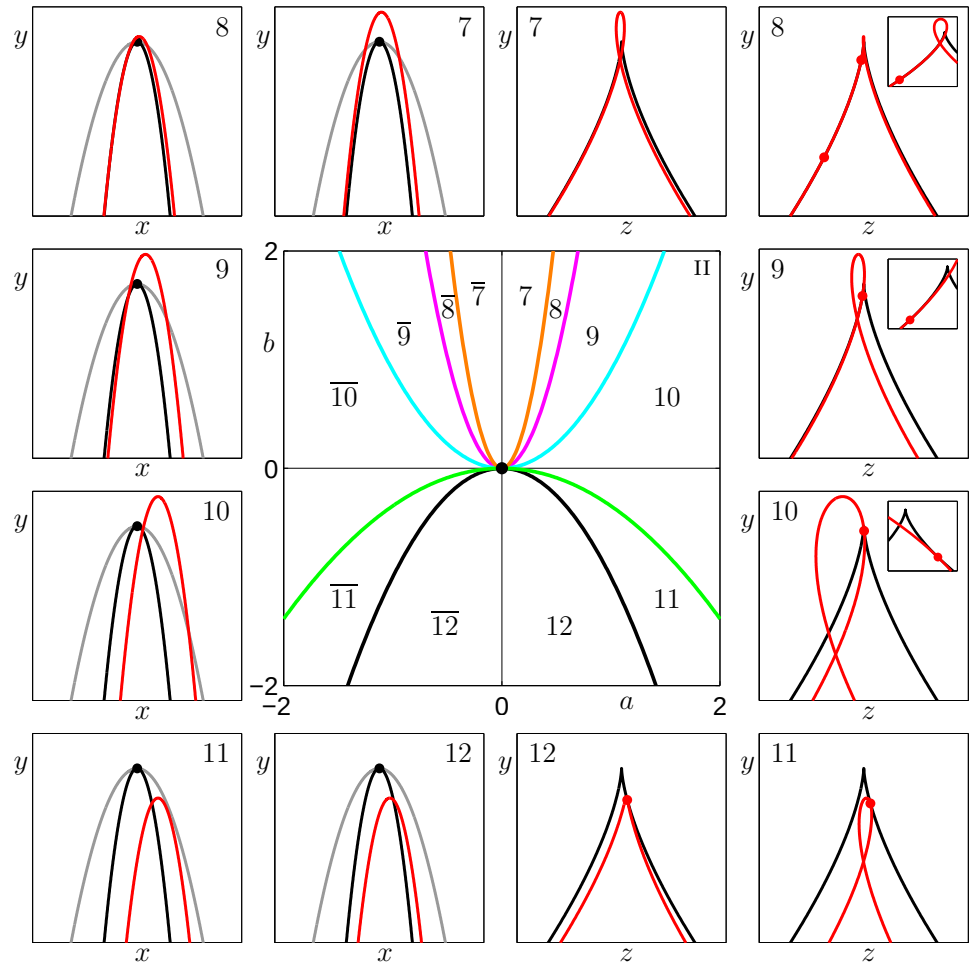

FIG. 5.4. Case II: $-1 < \gamma < -\frac{2}{3}$
The two-parameter unfolding in the (a, b)-plane with the bifurcation curves C (blue), L (black), I (purple), T (orange), and E (green); compare with Figs. 4.1 and 4.2. Representative phase portraits near C_0 are presented anti-clockwise from the second image at the top, and near C_1 clockwise from the third image at the top; shown are W and $F(W)$ (red curves), J_0 and J_1 (black curves), and $\widehat{J}_0$ (grey curve). The data is for $\gamma = -0.9$, with phase portraits for $(a, b) = (0.2, 1.7)$, $(a, b) = (0.2, 0.3)$, $(a, b) = (0.8, 1.7)$, $(a, b) = (2.0, 1.7)$, $(a, b) = (2.0, -1.7)$, and $(a, b) = (1.0, -1.7)$, respectively.

1.

Proof. According to Propositions 4.2 and 4.3, the points $\gamma = -1$, $\gamma = -\frac{1}{3}$, $\gamma = -\frac{1}{4}$, and $\gamma = 0$ give rise to topological changes of phase portraits and, hence, neighboring two-parameter unfoldings in the (a, b)-plane. It follows from (4.1) and (4.3) that $c_C(\gamma)$ and $c_I(\gamma)$ intersect at $\gamma = -\frac{1}{2}$, where the cusp transition and the intersection-at-tangency bifurcation change their order. Similarly, from (4.1) and (4.2), $c_C(\gamma)$ and $c_L(\gamma)$ intersect at $\gamma = 1$, where the cusp transition and the loop creation change their order. Finally, from (4.3) and (4.4) we conclude that $c_I(\gamma)$ is tangent to $c_T(\gamma)$ at $\gamma = -\frac{2}{3}$. This means that the intersection-at-tangency happens at a double-tangency point on J_1. Therefore, the intersection at $\gamma = -\frac{2}{3}$ is a genuine codimension-two

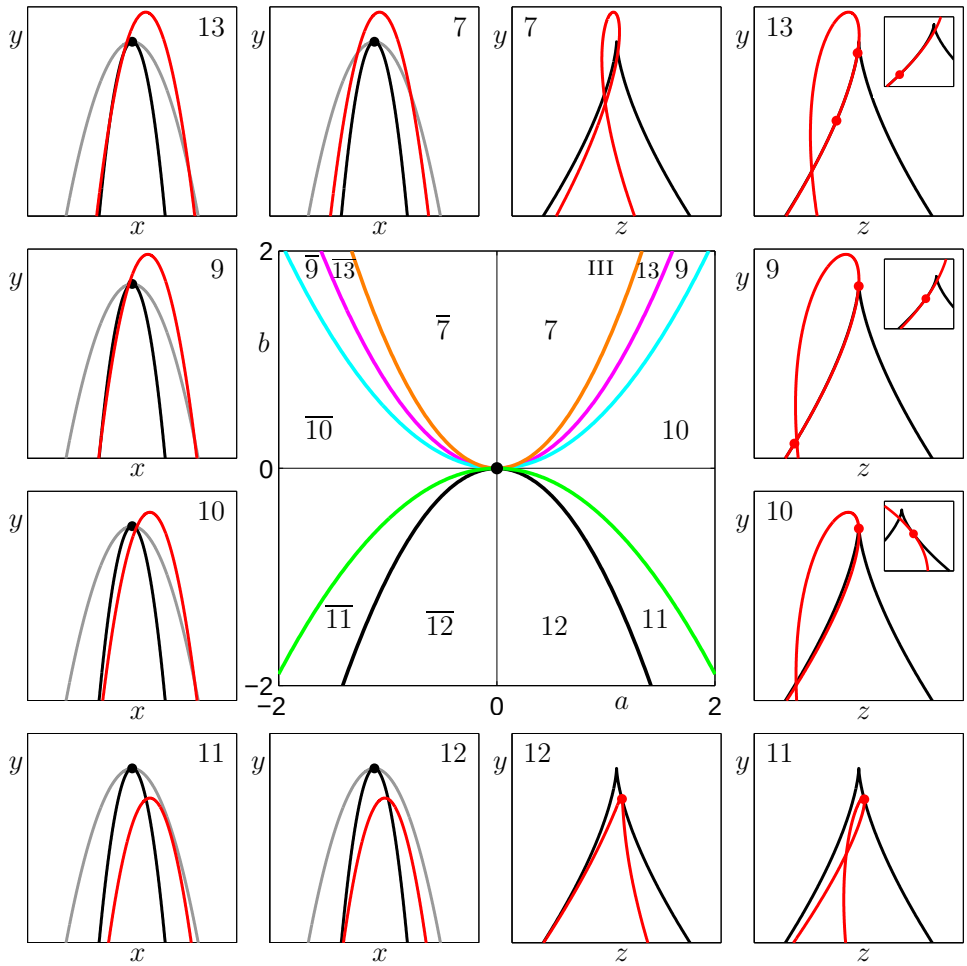

FIG. 5.5. Case III: $-\frac{2}{3} < \gamma - \frac{1}{2}$
The two-parameter unfolding in the (a, b)-plane with the bifurcation curves C (blue), L (black), I (purple), T (orange), and E (green); compare with Figs. 4.1 and 4.2. Representative phase portraits near C_0 are presented anti-clockwise from the second image at the top, and near C_1 clockwise from the third image at the top; shown are W and $F(W)$ (red curves), J_0 and J_1 (black curves), and $\widehat{J}_0$ (grey curve). The data is for $\gamma = -0.53$, with phase portraits for $(a, b) = (0.5, 1.7)$, $(a, b) = (1.3, 1.7)$, $(a, b) = (1.5, 1.7)$, $(a, b) = (1.7, 0.8)$, $(a, b) = (1.7, -1.7)$, and $(a, b) = (1.0, -1.7)$, respectively.

point that leads to a topological change in the phase portraits. Indeed, for (a, b) in between the tangency-creation and intersection-at-tangency bifurcation curves, the self-intersection of $F(W)$ lies closer to C_1 than the two tangencies of $F(W)$ with J_1 if $\gamma < -\frac{2}{3}$, while it lies furthest away from C_1 if $\gamma > -\frac{2}{3}$; compare phase portraits 8 and 13 in Figs. 5.4 and 5.5, respectively. □

The individual two-parameter unfoldings I–VIII in the (a, b)-plane are shown individually in Figs. 5.3 to 5.10. In each figure, the middle panel shows how the colored codimension-two bifurcation curves of Proposition 4.1 divide the (a, b)-plane into regions of topologically different phase portraits. The surrounding panels on the left show the respective configurations of W in a neighborhood of C_0 and those on the

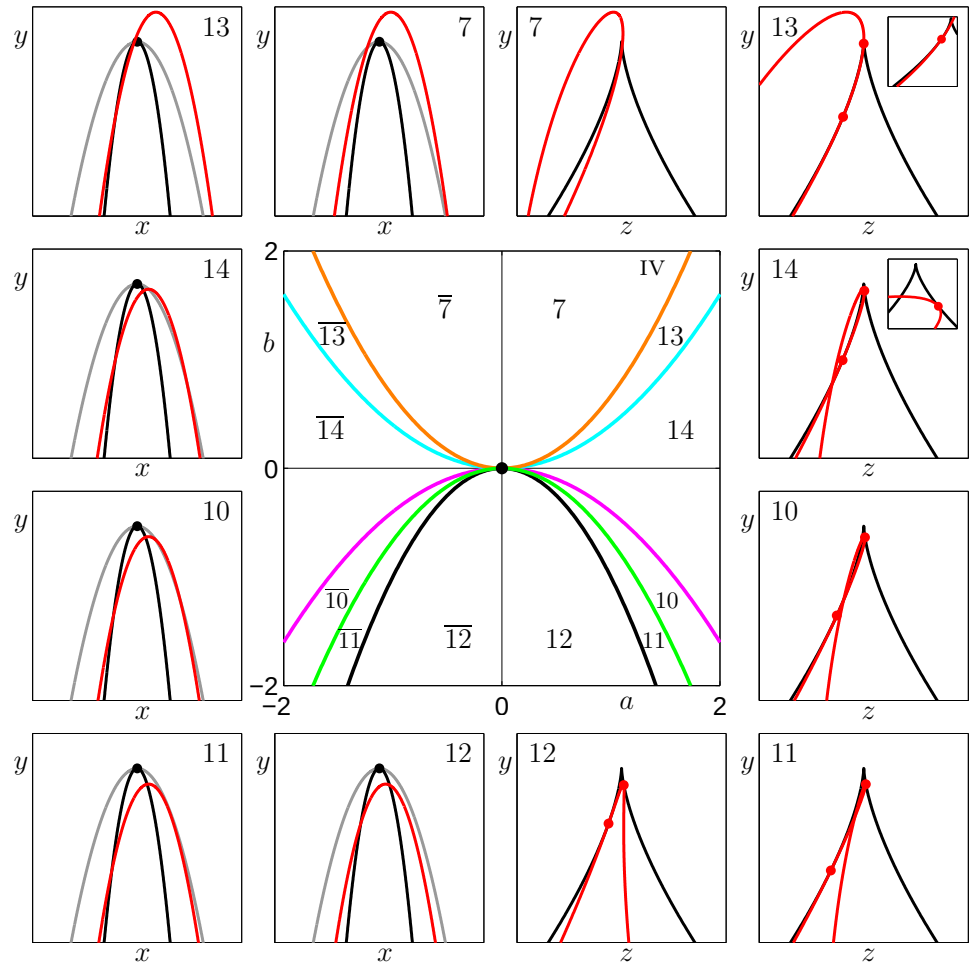

Fig. 5.6. Case iv: $-\frac{1}{2} < \gamma < -\frac{1}{3}$
The two-parameter unfolding in the (a, b)-plane with the bifurcation curves C (blue), L (black), I (purple), T (orange), and E (green); compare with Figs. 4.1 and 4.2. Representative phase portraits near C_0 are presented anti-clockwise from the second image at the top, and near C_1 clockwise from the third image at the top; shown are W and $F(W)$ (red curves), J_0 and J_1 (black curves), and $\widehat{J}_0$ (grey curve). The data is for $c = -0.4$, with phase portraits for $(a, b) = (1.1, 1.7)$, $(a, b) = (1.8, 1.7)$, $(a, b) = (1.1, -0.3)$, $(a, b) = (1.1, -0.6)$, $(a, b) = (1.1, -0.9)$, and $(a, b) = (0.6, -0.9)$, respectively.

right that of $F(W)$ in a neighborhood of C_1. Both the bifurcation curves and the configurations of W and $F(W)$ were drawn in Matlab directly from their respective formulas. In this way, one gets an impression of actual shapes and sizes. The disadvantage is that it is difficult to locate exactly where tangencies occur, which is why they have been highlighted (from their formula) with red dots. Where necessary, insets provide enlargements of how $F(W)$ lies relative to J_1. All phase portraits shown in Figs. 5.3 to 5.10 are for $a > 0$, as was the case for the sketches in Fig. 5.2. Note that crossing the line $a = 0$ above or below all bifurcation curves does not constitute a bifurcation, so that the respective phase portraits must be invariant under conjugation. The fact that this is indeed the case is evidence of the consistency of the

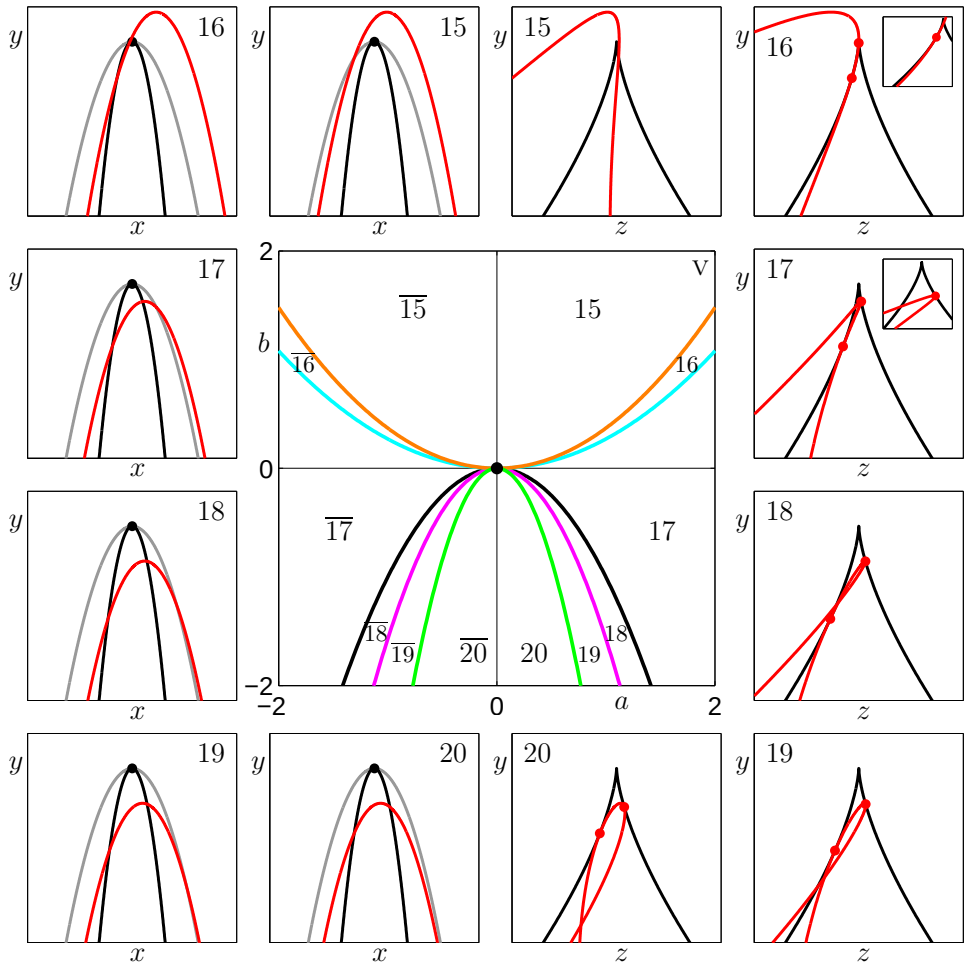

FIG. 5.7. Case V: $-\frac{1}{3} < \gamma < -\frac{1}{4}$
The two-parameter unfolding in the (a, b)-plane with the bifurcation curves C (blue), L (black), I (purple), T (orange), and E (green); compare with Figs. 4.1 and 4.2. Representative phase portraits near C_0 are presented anti-clockwise from the second image at the top, and near C_1 clockwise from the third image at the top; shown are W and $F(W)$ (red curves), J_0 and J_1 (black curves), and $\widehat{J}_0$ (grey curve). The data is for $\gamma = -0.27$, with phase portraits for $(a, b) = (1.2, 1.7)$, $(a, b) = (2.3, 1.7)$, $(a, b) = (1.2, -1.0)$, $(a, b) = (1.2, -2.0)$, $(a, b) = (1.0, -2.0)$, and $(a, b) = (0.6, -2.0)$, respectively.

unfoldings in Figs. 5.3 to 5.10.

As mentioned, the phase portraits for $a < 0$ can be obtained by conjugation, but a conjugate phase portrait may be topologically equivalent to a different phase portrait for $a > 0$. The following phase portraits do not result in topologically new phase portraits under conjugation with respect to the original list of 32 for $a > 0$ in Fig. 5.2.

- invariant under conjugation: 1, 6, 7, 12, 15, 20, 21, 26, and 31.
- identities under conjugation: $\overline{22} = 27$, $\overline{23} = 28$, and $\overline{24} = 29$.

As a result, there are 17 new classes of phase portraits that one obtains under conju-

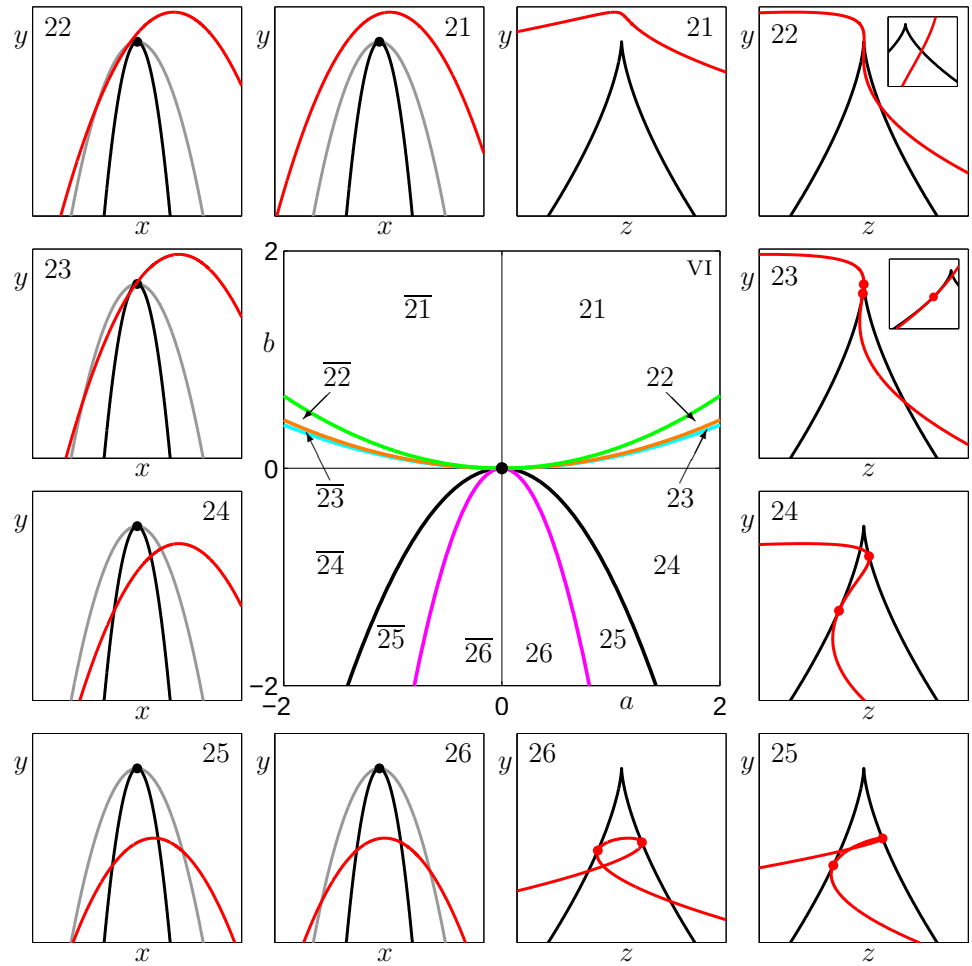

FIG. 5.8. Case VI: $-\frac{1}{4} < \gamma < 0$
The two-parameter unfolding in the (a, b)-plane with the bifurcation curves C (blue), L (black), I (purple), T (orange), and E (green); compare with Figs. 4.1 and 4.2. Representative phase portraits near C_0 are presented anti-clockwise from the second image at the top, and near C_1 clockwise from the third image at the top; shown are W and $F(W)$ (red curves), J_0 and J_1 (black curves), and $\widehat{J}_0$ (grey curve). The data is for $\gamma = -0.1$, with phase portraits for $(a, b) = (1.0, 1.7)$, $(a, b) = (3.5, 1.7)$, $(a, b) = (4.0, 1.7)$, $(a, b) = (4.0, -1.0)$, $(a, b) = (1.6, -4.0)$, and $(a, b) = (0.5, -4.0)$, respectively.

gation from the original list for $a > 0$, namely

- $\overline{2}$, $\overline{3}$, $\overline{4}$, $\overline{5}$, $\overline{8}$, $\overline{9}$, $\overline{10}$, $\overline{11}$, $\overline{13}$, $\overline{14}$, $\overline{16}$, $\overline{17}$, $\overline{18}$, $\overline{19}$, $\overline{25}$, $\overline{30}$, and $\overline{32}$.

This means that there are a total of 51 topologically different phase portraits according to Definition 3.4. If one chooses to consider conjugate phase portraits to be the same, that is, one does not distinguish between the two parts of J_1 (either side of the cusp point) on which the intersections and tangencies occur, then there are a total of 29 phase portraits.

5.1. Relevance of normal-form unfoldings. The map F is the normal form for any endomorphism f in a sufficiently small neighborhood of a generic cusp point

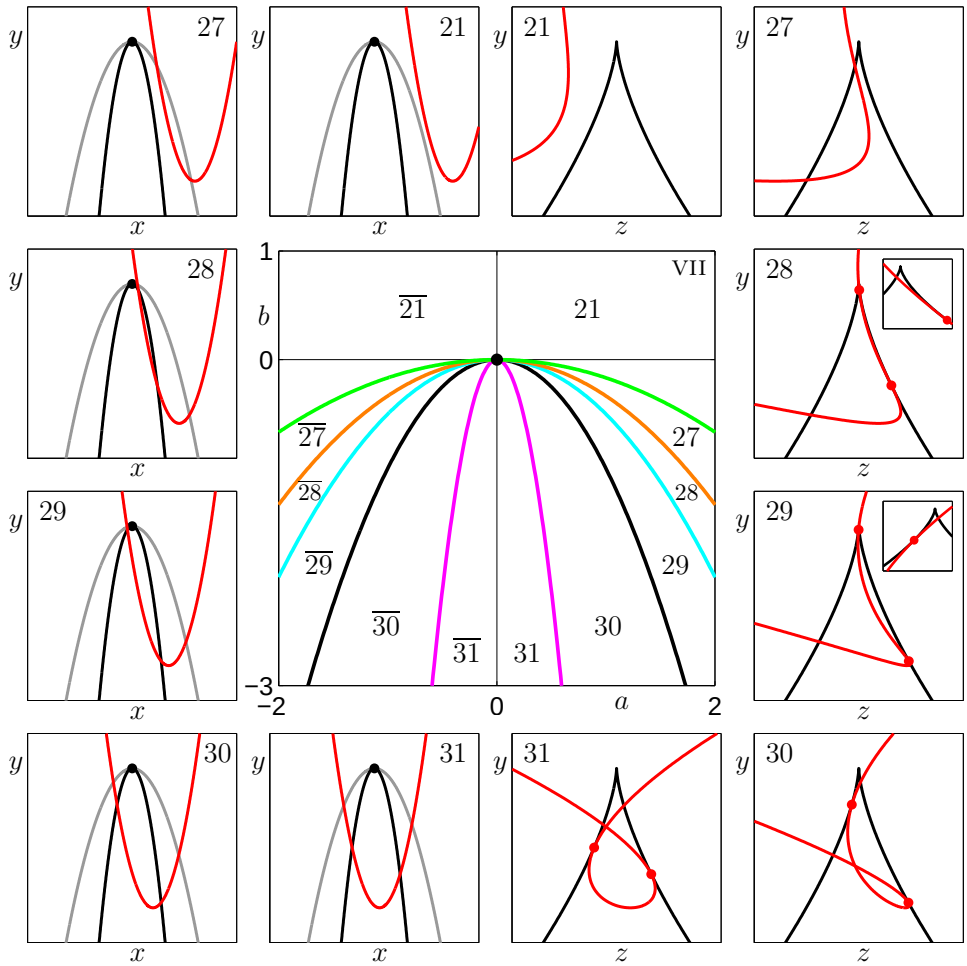

FIG. 5.9. Case VII: $0 < \gamma < 1.0$
The two-parameter unfolding in the (a, b)-plane with the bifurcation curves C (blue), L (black), I (purple), T (orange), and E (green); compare with Figs. 4.1 and 4.2. Representative phase portraits near C_0 are presented anti-clockwise from the second image at the top, and near C_1 clockwise from the third image at the top; shown are W and $F(W)$ (red curves), J_0 and J_1 (black curves), and $\widehat{J}_0$ (grey curve). The data is for $\gamma = 0.5$, with phase portraits for $b = -8.0$ and $a = 7.5$, $a = 6.0$, $a = 4.5$, $a = 3.5$, $a = 2.0$, and $a = 0.5$, respectively.

C_1 on J_1. Furthermore, at the cusp-cusp bifurcation the tangency of the smooth invariant curve W with J_0 at the pre-cusp point is quadratic. Therefore, we have the following.

COROLLARY 5.2. *Consider a family of planar endomorphisms f_λ with a cusp-cusp bifurcation at the parameter point $(\lambda_1^*, \lambda_2^*)$, that is, a quadratic tangency of an invariant curve W to a pre-cusp point C_0 on J_0. Then there exist sufficiently small neighborhoods U of C_0 and V of the cusp point $C_1 = f(C_0)$ such that*

1. *The parameters λ_1 and λ_2 generically unfold the cusp-cusp bifurcation in a sufficiently small neighborhood Λ of $(\lambda_1^*, \lambda_2^*)$. Each of the cases* I–VIII *of two-parameter unfoldings may occur as the bifurcation diagram of f in V for*

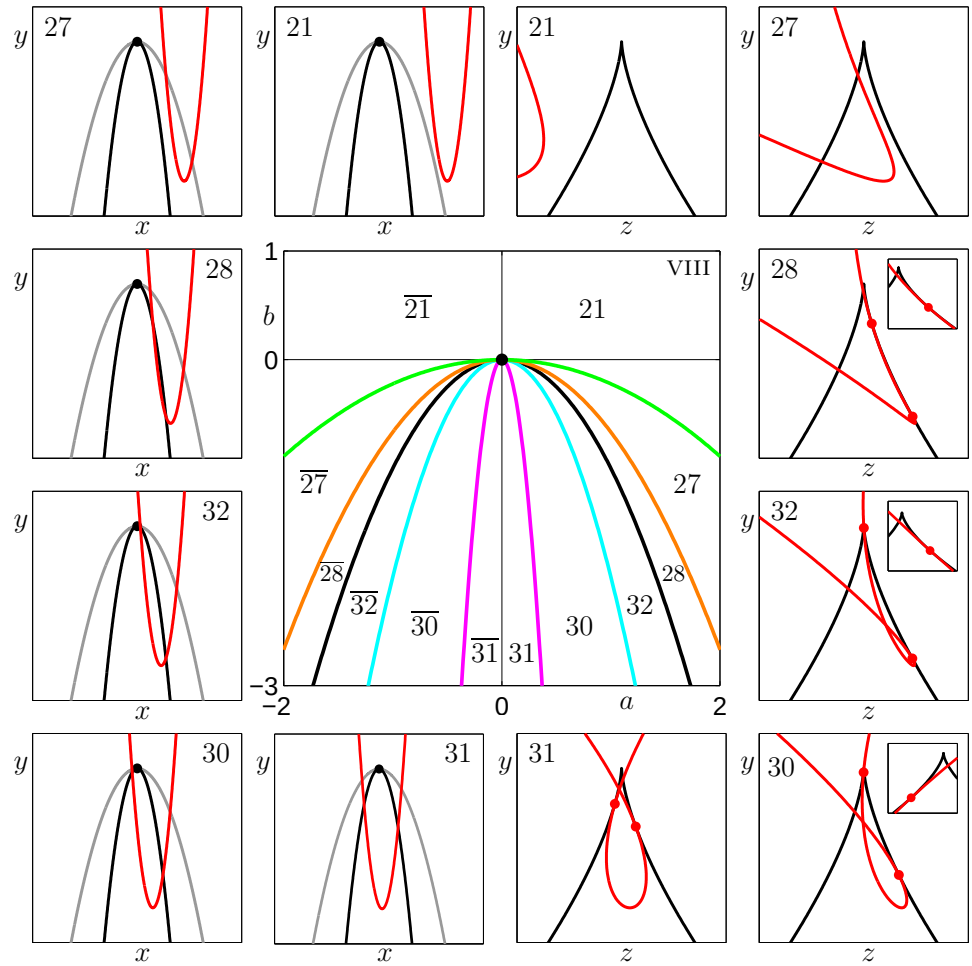

FIG. 5.10. Case VIII: $1.0 < \gamma < \infty$
The two-parameter unfolding in the (a, b)-plane with the bifurcation curves C (blue), L (black), I (purple), T (orange), and E (green); compare with Figs. 4.1 and 4.2. Representative phase portraits near C_0 are presented anti-clockwise from the second image at the top, and near C_1 clockwise from the third image at the top; shown are W and $F(W)$ (red curves), J_0 and J_1 (black curves), and $\widehat{J}_0$ (grey curve). The data is for $\gamma = 2.0$, with phase portraits for $b = -8.0$ and $a = 6.5$, $a = 4.5$, $a = 3.2$, $a = 2.3$, $a = 1.5$, and $a = 0.3$, respectively.

$(\lambda_1, \lambda_2) \in \Lambda$. *In particular, all respective classes of phase portraits can be found in* V.

2. *Which case of unfolding occurs depends on the exact position of the two-jet of the curve* W *at the cusp-cusp bifurcation relative to the normal form coordinate systems generated by the two-jets of* J_0 *and* $\widehat{J}_0$.

Proof. Consider the coefficient of the two-jet of W at C_0 relative to the normal form coordinate systems generated by the two-jets of J_0 and $\widehat{J}_0$. If this coefficient lies in one of the open regions representing cases I–VIII, then this is an open condition. Since the two-jet of W depends continuously on (λ_1, λ_2), its coefficient does not leave the respective open region for $(\lambda_1^*, \lambda_2^*)$ as long as Λ is a sufficiently small neighborhood.

Furthermore, generically the map from (λ_1, λ_2) to (a, b) is a local diffeomorphism. Hence, generically, (λ_1, λ_2) unfolds the cusp-cusp bifurcation. □

Proposition 5.2 is in the spirit of local bifurcation theory: it states that the generic open regions corresponding to cases I–VIII are stable under perturbation of the purely quadratic character of the normal form, so that they must be expected in practical situations. Note also that, no matter which case of unfolding occurs, the five codimension-one bifurcations of Proposition 4.1 are, generically, part of the bifurcation diagram of f in V. When λ_1 and λ_2 are changed outside Λ then an intersection or (generic) tangency of $f(W)$ with J_1 may leave the neighborhood V. This corresponds to bifurcations at infinity; see Proposition 4.2.

The open regions of the normal-form setting are stable under perturbation, but this may or may not be true for the boundaries between them; see Fig. 5.1. First of all we expect the tangency between the curves $c_I(\gamma)$ and $c_T(\gamma)$ at $\gamma = -\frac{2}{3}$ to be preserved under perturbations, because it corresponds to a genuine codimension-two bifurcation, namely a simultaneous tangency-creation and intersection-at-tangency bifurcation. On the other hand, the tangency between the curves $c_E(\gamma)$, $c_T(\gamma)$ and $c_C(\gamma)$ at $\gamma = 0$ should be destroyed by generic perturbations. However, as follows from the definition of the bifurcations involved, the order of the bifurcations cannot change. Similarly, we expect that the tangency between the curves $c_E(\gamma)$ and $c_I(\gamma)$ at $\gamma = -\frac{1}{3}$ exactly at the intersection with $c_L(\gamma)$ will be destroyed, while the order of the curves $c_E(\gamma)$ and $c_I(\gamma)$ will be maintained. Overall, new regions may be created that feature phase portraits that do not occur in the normal form. However, because the invariant curve W is assumed to have a quadratic tangency (which is a generic assumption), the perturbation of the boundary curves in Fig. 5.1 is small and goes to zero as the cusp-cusp point $(\lambda_1^*, \lambda_2^*)$ is approached. In other words, sufficientlty close to $(\lambda_1^*, \lambda_2^*)$ one should expect to see 'only' the two-parameter unfoldings I–VIII presented here.

In any practical application of Proposition 5.2 it will be interesting to see how big the neighbourhoods Λ and V are. Indeed, the larger they can be chosen, the easier it is to identify the different types of phase portraits that must occur near the cusp-cusp bifurcation. In practice, it is possible to deduce which case one is dealing with by carefully finding the respective phase portraits in V, as we will see from the example in the next section.

6. Cusp-cusp bifurcation in an adaptive control system. As a concrete example we consider the one-dimensional first-order approximation of a linear, time-invariant, single-input single-output process with a unit time delay introduced in [9]. In this example, the plant contains an unknown parameter that must be estimated using input-output data available from previous time intervals. The objective is to design a controller that will track a constant nonzero reference signal. In non-dimensional form, this leads to the planar endomorphism

$$g : \begin{pmatrix} x \\ y \end{pmatrix} \mapsto \begin{pmatrix} -xy + \eta \\ \beta y + \frac{px(-yx+\eta-1)}{c+x^2} \end{pmatrix}, \tag{6.1}$$

where x is the output signal — which should equal 1 if the controller achieves its objective — and y corresponds to the estimation of the unknown parameter in the system. The parameter η corresponds to a constant disturbance on the system, and p is directly related to the adaptation gain. The parameters β and c determine the effectiveness of the feedback controller; $\beta = 1$ was used in [9]. The noninvertibility of the map is due to the time delay, or sampling time, when constructing the feedback.

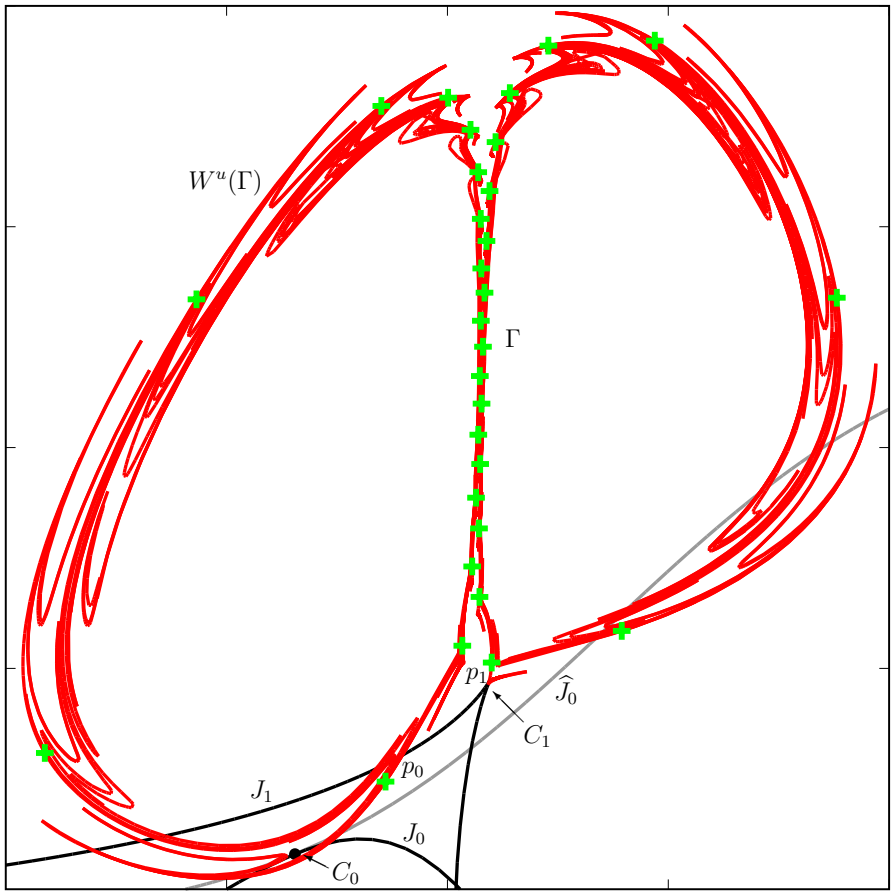

Fig. 6.1. Global phase portrait of the map g of (6.1) for $p = 0.81$, $c = 1.2$, $\gamma = -0.153$ and $\beta = 1.0005$. Shown is how the unstable manifold $W^u(\Gamma)$ of the saddle period-30 orbit Γ interacts with the curves J_0, $\widehat{J}_0$ and J_1. The situation is close to a cusp-cusp bifurcation, as is evidenced by how $W^u(\Gamma)$ approaches the cusp point C_1.

The three-parameter family with $\beta = 1$ was also studied in the tutorial paper [10], where it was shown that a saddle exists with an unstable manifold that interacts with a cusp on J_1. The phase portraits in [10] were a direct motivation for us to investigate the codimension-two bifurcation organizing this type of behaviour, namely the cusp-cusp bifurcation. Our study of the possible unfoldings in Sec. 4 indicates that the family (6.1) for $\beta = 1$ displays the arrangements of an invariant curve near a cusp point C_1 that can be found in unfolding vii. The respective phase portraits are part of a scenario that involves the unstable manifold of a period-30 orbit inside a resonance tongue in some appropriate parameter plane. Unfortunately, while this unstable manifold has a quadratic tangency with J_0 very close to the pre-cusp point C_0, it is not possible to vary the parameters such that the tangency occurs exactly at C_0 before leaving the narrow period-30 resonance tongue.

In order to find a cusp-cusp bifurcation for the family (6.1) it is necessary to vary β. Specifically, we consider the (η, β) plane for fixed $p = 0.81$ and $c = 1.2$. By starting at $(\eta, \beta) = (-0.14, 1.0)$, we found a cusp-cusp point at $(\eta, \beta) \approx (-0.14439095, 1.00181158)$.

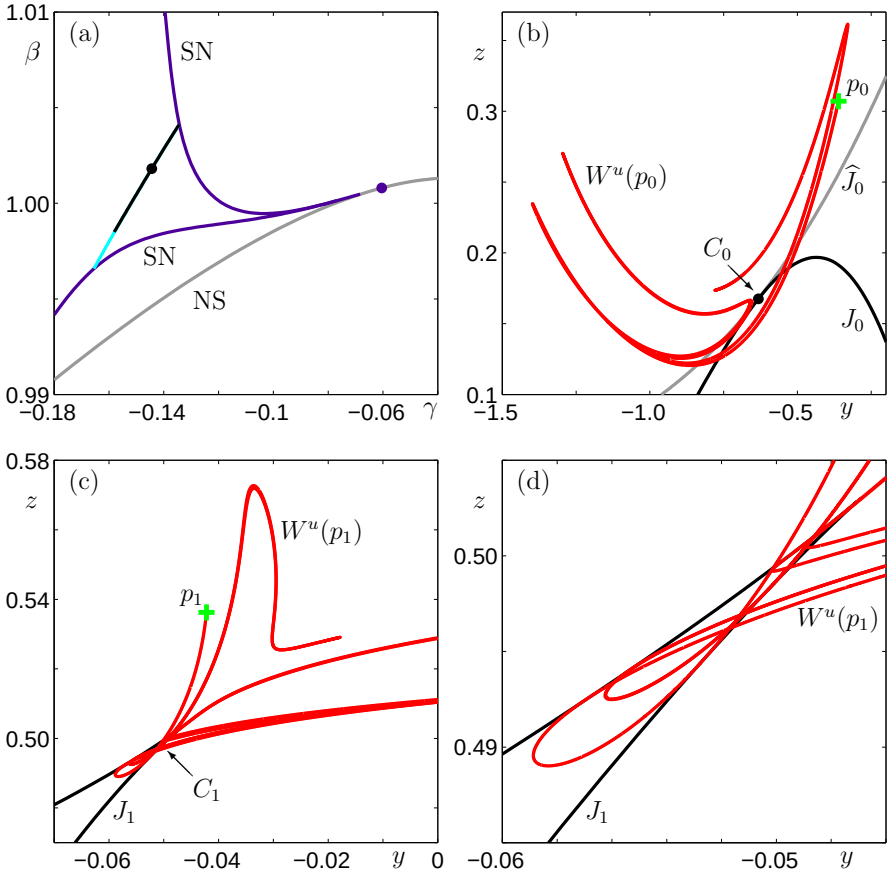

FIG. 6.2. Panel (a) shows the bifurcation diagram in the (η, β)-plane of (6.1) for fixed $p = 0.81$ and $c = 1.2$. Notice the period-30 resonance tongue emanating from a Neimarck-Sacher bifurcation NS and bounded by saddle-node curves SN. The curves C of cusp transition (black) and L of loop creation (blue) inside the tongue are tangent at a cusp-cusp bifurcation point (black dot). Panels (b)–(d) are for $(\eta, \beta) = (-0.153, 1.0005)$ and show enlargements of Fig. 6.1. The period-30 saddle p_0 and its unstable manifold $W^u(p_0)$ are shown in panel (b) near C_0. They map to p_1 and $W^u(p_1)$ under g, which are shown near C_1 in panels (c) and the enlargement of (d).

Figure 6.1 shows the general arrangement of the period-30 orbit Γ (green crosses) and its unstable manifold $W^u(\Gamma)$ (red curves) for $p = 0.81$, $c = 1.2$, $\eta = -0.153$ and $\beta = 1.0005$. Successive images on the orbit alternate from left to right, move up the middle of the figure, and then separate around the outsides. There are 15 points on each of the two 'circles' surrounding a period-2 orbit (not shown). Also shown are the curves J_0, $\widehat{J}_0$ and J_1; see also already Fig. 6.4 for the global arrangements of these curves. On the scale of Fig. 6.1 it appears that the system is very close to a quadratic tangency of $W^u(\Gamma)$ at the pre-cusp C_0 on J_0 and a resulting cusp-cusp singularity at C_1 on J_1. From Proposition 3.2 and Fig. 3.1 we conclude with the direction of cuspidal appearance of $W^u(\Gamma)$ near C_1 that we must expect an unfolding of either case VII or VIII.

As part of our subsequent analysis of (6.1) we computed the bifurcation diagram of Fig. 6.2(a) in the (η, β)-plane for fixed $p = 0.81$ and $c = 1.2$; see Appendix A for details

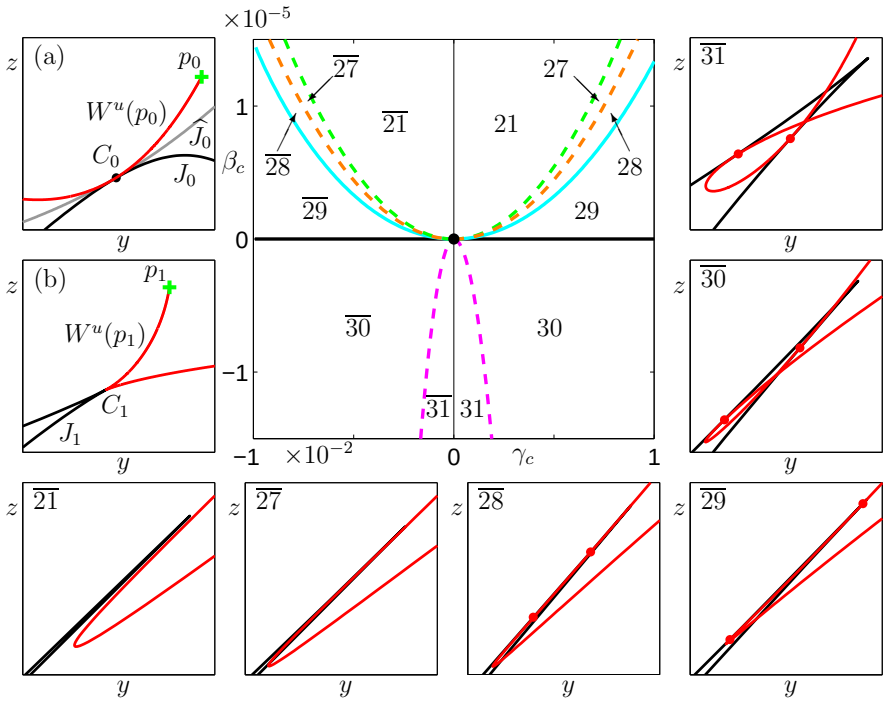

Fig. 6.3. The main panel is the bifurcation diagram in the (η_c, β_c)-plane for fixed $p = 0.81$ and $c = 1.2$, where η_c is the distance from the cusp point and β_c the β-distance from the curve C. In this representation the cusp-cusp bifurcation point, which was determined numerically to be at $(\eta, \beta) = (-0.14439095, 1.00181158)$, is at the origin. The solid curves C (blue) and L (black) were continued numerically, while the dashes curves I (purple), T (orange) and E (green) were found by a systematic exploration of the (η_c, β_c)-plane. In combination with the surrounding representative phase portraits (for $\eta_c < 0$), the bifurcation diagram can be identified as an unfolding of case vi. Panel (a) shows a global overview for $\gamma = -0.153$ and $\beta = 0.999727$ of $W^u(p_0)$ near C_0, and panel (b) of $W^u(p_1)$ near C_1. At this scale panels (a) and (b) are quite representative for all regions of the bifurcation diagram. The exact structure of the interaction of $W^u(p_1)$ with J_1 only comes to light in the enlargements shown in the other panels, which are for $\gamma = -0.153$ and $\beta = 0.999727$ (case $\overline{21}$), $\beta = 0.999729$ (case $\overline{27}$), $\beta = 0.999732$ (case $\overline{28}$), $\beta = 0.999738$ (case $\overline{29}$), $\beta = 0.9998$ (case $\overline{30}$), and $\beta = 1.0005$ (case $\overline{31}$).

of the numerical algorithms. Figure 6.2(a) shows a curve, NS, of Neimarck-Sacker bifurcations along which a torus bifurcates. The resonance tongue of the period-30 orbit emanates from a resonance point on NS and is bounded by two saddle-node bifurcations of periodic orbits, denoted SN. Shown in black is the curve L of loop-creation, which is very close to the blue curve C of cusp transition. The black dot is the codimension-two cusp-cusp point, where these two codimension-one curves are tangent. To obtain the phase portraits relating to the cusp-cusp bifurcation, one needs to identify a relevant part of the unstable manifold $W^u(\Gamma)$. These are the lower left branch of the unstable manifold $W^u(p_0)$ of the point $p_0 \in \Gamma$, and its image, the lower left branch of $W^u(p_1)$ of the point $p_1 = g(p_0) \in \Gamma$. Portions of these two local manifolds are shown in relation to J_0 and J_1 in Fig. 6.2(b) and (c), respectively for the case $(\eta, \beta) \approx (-0.153, 1.0005)$ from Fig. 6.1.

Note from Fig. 6.2(b) that $W^u(p_0)$ makes a number of close passes 'around' C_0. This explains that Fig. 6.2(d) shows several invariant curves locally near C_1 that all

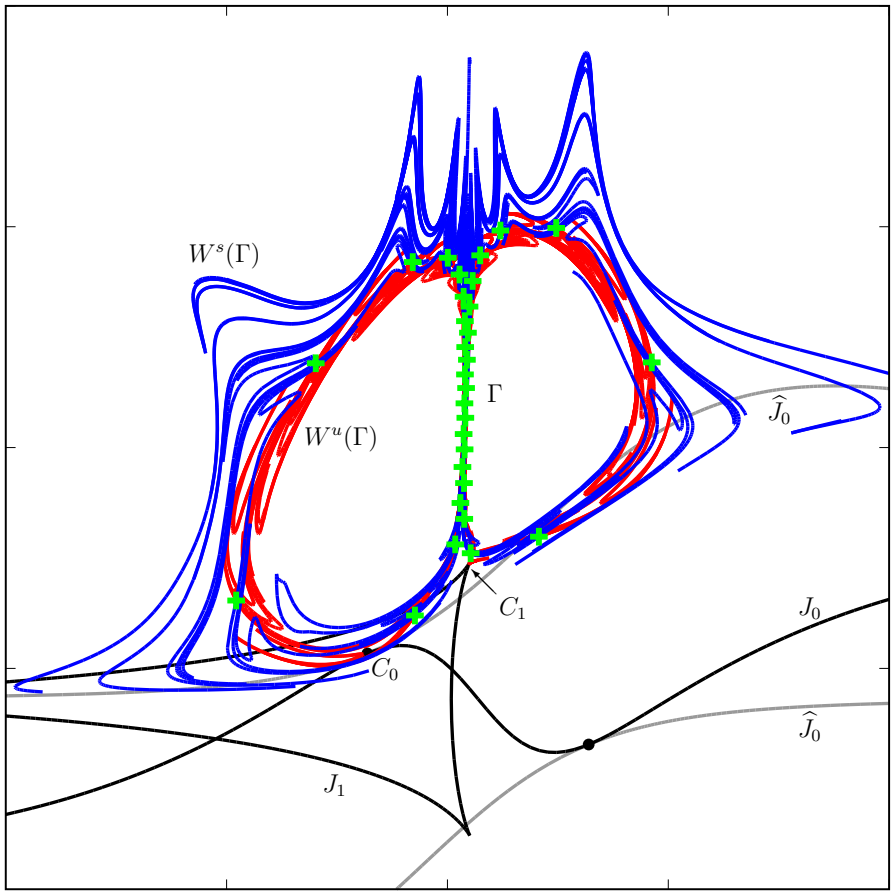

FIG. 6.4. Global phase portrait of the map g of (6.1) for $p = 0.81$, $c = 1.2$, $\gamma = -0.153$ and $\beta = 1.0005$, showing also the stable set $W^s(\Gamma)$ of the period-30 orbit Γ; compare with Fig. 6.1.

form loops as in phase portrait 31, namely one loop for each 'pass' of $W^u(p_0)$ around C_0; When parameters are changed, it appears possible to create further cusp-cusp points, namely at tangencies of different segments of $W^u(p_0)$ with J_0 at C_0.

In Fig. 6.3 we show the numerically obtained unfolding of the 'first' such cusp-cusp bifurcation point, where $W^u(p_0)$ has a quadratic tangency with J_0 and $\widehat{J}_0$ at the pre-cusp point C_0 as its first entry into a neighborhood of C_0; see panel (a). The cusp-cusp bifurcation was determined numerically as $(\eta, \beta) \approx (-0.14439095, 1.00181158)$. The central panel shows the bifurcation diagram around this point in the (η_c, β_c)-plane, where η_c is the distance from the cusp point in the η-direction and β_c is defined as the distance in the β-direction from the curve C. In this representation the curve C appears as the horizontal η_c-axis and the cusp-cusp singularity is at the origin, and this allows for a good comparison with the two-parameter unfoldings of the normal-form setting. Notice the largely differing scales of the axes, which corresponds to the fact that the curves C (blue) and L (black) are very close to each other; compare with Fig. 6.2(a). The remaining curves I, T and E are sketched in Fig. 6.3, because they have not been found directly. Rather, they were determined indirectly by a careful examination of the (η_c, β_c)-plane. Indeed their existence can be deduced from the

existence of the respective phase portraits of $W^u(p_1)$ relative to J_1 near the cusp point C_1, which are shown in the surrounding panels of Fig. 6.3. Overall we conclude that the unfolding of the cusp-cusp bifurcation in Fig. 6.3 is topologically as case VII in Fig. 5.9.

We finish by showing in Fig. 6.4 a global view of the period-30 saddle orbit Γ of g with is unstable manifold $W^u(\Gamma)$ as well as its stable set $W^s(\Gamma)$. Notice how the complicated structure of homoclinic and heteroclinic orbits interacts with J_1, including the cusp point C_1. It is this interplay between features of diffeomorphisms and the folding nature due to noninvertibility that is responsible for the interest in the break-up of invariant curves of endomorphisms; see, for example, [10, 11, 23, 25, 21]. It should be clear from Fig. 6.4 that many interesting questions remain for future research.

7. Conclusions. In this paper we have identified and analyzed a codimension-two bifurcation — the cusp-cusp bifurcation — that arises in generic planar endomorphisms f. This bifurcation is due to the feature of folding of the phase plane along the singular curve J_0. Its image J_1 generically has isolated cusp points, which are associated with pre-cusp points on J_0 where the eigenvector of the eigenvalue zero of the Jacobian Df is tangent to the curve J_0. The cusp-cusp bifurcation occurs when an invariant curve W is tangent to J_0 exactly at a pre-cusp point C_0. This forces the images $f(W)$ of the invariant curve to have a cusp exaclty at the cusp point C_1 on J_1.

Under perturbation, the cusp point C_1 on J_1 persists, but the image $f(W)$ may have many different configurations relative to C_1 and J_1. We chose to define an equivalence relation between two phase portraits in terms of ordered 'generic events' along the image of the invariant curve $f(W)$ (see Definitions 3.3 and 3.4. In particular, the codimension-one bifurcations, of which there are five, can be defined rigorously. Our definition makes equivalences easy to verify in specific examples and applications. In particular, it agrees with the distinctions between the different phase portraits and the descriptions of codimension-one bifurcations that have been reported in the literature. Specifically, in the adaptive control example we presented it was straightforward to establish the equivalence of the observed phase images with the respective normal-form unfolding. The technical challenge here was to achieve numerically the required resolution of J_1 and the unstable manifold segments.

All possible phase portraits in a local neighborhood of C_1 are organized into eight different classes of two-parameter unfoldings. Which case occurs depends on the relative curvature of W and J_0 at the bifurcation point. We presented these unfolding and the associated 32 classes of phase portraits (with an additional 17 that may be obtained by conjugation). Our approach has been to represent the quadratic tangency of W with J_0 at C_0 by a parabola of a given steepness, which is a suitable approximation in a small enough neighborhood of the cusp-cusp point. In combination with the normal form of a map with a cusp singularity this allowed us to introduce a normal form setting of the codimension-two bifurcation. The unfolding parameters in this setting are the horizontal and vertical positions of the maximum or minimum of the parabola (a and b in (3.1)), where J_0 is a horizontal line and C_0 is at the origin. The relative curvature of the parabola W is represented by the quadratic coefficient γ. Depending on the value of γ, we found the eight cases I–VIII. The main results in the paper are represented and illustrated by the division of the γ-line in Fig. 5.1, the list of possible phase portraits in Fig. 5.2 and the images of the eight unfoldings in Figs. 5.3 through 5.10. How these unfoldings manifest themselves in a practical

example was demonstrated with a planar, noninvertible model from adaptive control.

Within the theoretical and numerical framework presented here, it should be possible to locate and continue the respective bifurcation curves in a variety of examples, even noninvertible maps without a cusp point on J_1. This means that one may encounter additional codimension-two bifurcations as organizing centers. As we have already briefly mentioned, new bifurcations — of codimension two and three — will also be associated with the boundaries between the different unfoldings presented here. We believe that new bifurcations of planar endomorphisms could be investigated using the same singularity tools utilised in this paper.

Finally, we mention endomorphisms with phase spaces of dimension larger than two, of which there are hardly any examples in the literature. The reason seems to be that the way phase space is folded is much more complicated and particularly difficult to visualize. We believe that the bifurcation analysis of such noninvertible dynamical systems can only be tackled effectively with tools from singularity theory in the spirit of the study presented here. This presents an interesting and serious challenge for future research.

Acknowledgments. We thank Yannis Kevrekidis for helpful discussions. B.K. and H.M.O. were both supported by EPSRC Advanced Research Fellowship grants. B.B.P. acknowledges support from the National Science Foundation (grant #DMS-9973926) and the hospitality and support of the Bristol Centre for Applied Nonlinear Mathematics during his sabbatical in Fall 2004.

REFERENCES

[1] R. A. Adomaitis, and I. G. Kevrekidis, *Noninvertibility and structure of basins of attraction in a model adaptive control system*, J. Nonlin. Sci., 1 (1991), pp. 95–105.

[2] A. Agliari, *Global bifurcations in the basins of attraction in noninvertible maps and economic applications*, Nonlin. Anal., 47(8) (2000), pp. 5241–5252.

[3] A. Agliari, L.Gardini, and C. Mira, *On the fractal structure of basin boundaries in two-dimensional noninvertible maps*, Internat. J. Bifur. Chaos Appl. Sci. Engrg., 13(7) (2003), pp. 1767–1785.

[4] V. I. Arnol′d , *Catastrophe Theory*, 3rd ed., Springer-Verlag, Berlin, 1992.

[5] H. W. Broer, M. Golubitsky. and G. Vegter, *The geometry of resonance tongues: a singularity theory approach*, Nonlinearity, 16(4) (2003), pp. 1511–1538.

[6] J. P. England, B. Krauskopf, and H. M. Osinga, *Computing one-dimensional stable manifolds of planar maps without the inverse*, SIAM J. Appl. Dyn. Syst., 3(2) (2004), pp. 161–190.

[7] J. P. England, B. Krauskopf, and H. M. Osinga, *Bifurcations of stable sets in noninvertible planar maps*, Internat. J. Bifur. Chaos Appl. Sci. Engrg., 15(3) (2005), pp. 891–904.

[8] C. E. Frouzakis, R. A. Adomaitis, and I. G. Kevrekidis, *An experimental and computational study of subcriticality, hysteresis and global dynamics for a model adaptive control system*, Comp. Chem. Engng., 120 (1996), pp. 1029–1034.

[9] C. E. Frouzakis, R. A Adomaitis, and I. G. Kevrekidis, M. P. Golden, and B. E. Ydstie, *The structure of basin boundaries in a simple adaptive control system*, in Chaotic Dynamics: Theory and Practice, T. Bountis (ed.), Plenum Press, New York, 1992, pp. 195-210.

[10] C. E. Frouzakis, L. Gardini, I. G. Kevrekidis, G. Millerioux, and C. Mira, *On some properties of of invariant sets of two-dimensional noninvertible maps*, Internat. J. Bifur. Chaos Appl. Sci. Engrg., 7(6) (1997), pp. 1167–1194.

[11] C. E. Frouzakis, I. G. Kevrekidis, and B. B. Peckham, *A route to computational chaos revisited: noninvertibility and the breakup of an invariant circle*, Phsys. D, 177 (2003), pp. 101–121.

[12] M. Golubitsky and D. G. Shaeffer, *Singularities and Groups in Bifurcation Theory*, Vol. 1, Springer-Verlag, New York, 1985.

[13] J. Guckenheimer and P. Holmes, *Nonlinear Oscillations, Dynamical Systems, and Bifurcations of Vector Fields*, Springer-Verlag, New York, Berlin, 1983.

[14] I. GUMOWSKI AND C. MIRA, *Dynamique Chaotique*, Cepadues Éditions, Toulouse, 1980.
[15] I. GUMOWSKI AND C. MIRA, *Recurrences and Discrete Dynamic Systems*, Springer-Verlag, New York, 1980.
[16] M. HÉNON, *A two-dimensional mapping with a strange attractor*, Commun. Math. Phys., 50(1) (1976), pp. 69–77.
[17] K. IKEDA *Multiple-valued stationary state and its instability of the transmitted light from a ring cavity system*, Optics Communications, 30 (1979), pp. 257–261.
[18] H. KITAJIMA, H. KAWAKAMI, AND C. MIRA, *A method to calculate basin bifurcation sets for a two-dimensional noninvertible map*, Internat. J. Bifur. Chaos Appl. Sci. Engrg., 10(8) (2000), pp. 2001–2014.
[19] B. KRAUSKOPF AND H. M. OSINGA, *Growing 1D and quasi-2D unstable manifolds of maps*, J. Comput. Phys., 146 (1998), pp. 406–419.
[20] B. KRAUSKOPF AND C. ROUSSEAU, *Codimension-three unfoldings of reflectionally symmetric planar vector fields*, Nonlinearity, 10(5) (1997), pp. 1115–1150.
[21] E. N. LORENZ, *Computational chaos — a prelude to computational instability*, Physica D, 35 (1989), pp. 299–317.
[22] V. MAISTRENKO, YU. MAISTRENKO, AND I. SUSHKO, *Noninvertible two-dimensional maps arising in radiophysics*, Internat. J. Bifur. Chaos Appl. Sci. Engrg., 4(2) (1996), pp. 383–400.
[23] V. MAISTRENKO, YU. MAISTRENKO, AND E. MOSEKILDE, *Torus breakdown in noninvertible maps*, Phys. Rev. E, 67 (2003), 046215.
[24] C. MIRA, C. JEAN-PIERRE, G. MILLÉRIOUX, AND L. GARDINI, *Plane foliation of two-dimensional noninvertible maps*, Internat. J. Bifur. Chaos Appl. Sci. Engrg., 6(8) (1996), pp. 1439–1462.
[25] C. MIRA, L. GARDINI, A. BARUGOLA, AND J. C. CATHALA, *Chaotic dynamics in two-dimensional noninvertible maps*, Nonlin. Sci. Series A, World Scientific, Singapore, 1996.
[26] C.-H. NIEN AND F. J. WICKLIN, *An algorithm for the computation of preimages in noninvertible mappings*, Internat. J. Bifur. Chaos Appl. Sci. Engrg., 8(2) (1998), pp. 415–422.
[27] J. PALIS AND W. DE MELO, *Geometric Theory of Dynamical Systems*, Springer-Verlag, New York, Berlin, 1982.
[28] B. B. PECKHAM, *To Be Continued ...*, Continuation and phase space software for discrete dynamical systems, `www.d.umn.edu/~bpeckham/tbc\_home.html` (1986-present).
[29] R. RICO-MARTINEZ, R. A. ADOMAITIS, AND I. G. KEVREKIDIS, *Noninvertibility in neural networks*, Comp. Chem. Engng., 24 (2000), pp. 2417–2433.
[30] M. SPIVAK, *A Comprehensive Introduction to Differential Geometry*, Vol 1, Publish or Perish, Inc., Houston, TX, 2nd ed., 1970, 1979.
[31] S. H. STROGATZ *Nonlinear dynamics and chaos: With applications to physics, biology, chemistry, and engineering*, Perseus Books, Reading, MA, Cambridge MA, 1994.
[32] H. WHITNEY, *On singularities of mappings of Euclidean spaces. I. Mappings of the plane into the plane*, Annals Math., 2nd Ser., Vol. 62(3) (1955), pp. 374–410.

Appendix A. Numerical methods.

The unstable manifolds in Figs. 6.1 and 6.4 (red curves) were computed with the method from [19]. The stable sets shown in Figs. 6.4 (blue curves) were computed with the Search Circle algorithm introduced in [6], which does not require the inverse of the map. In fact, shown are the primary manifolds of the 30 periodic points, that is, the unique pieces of the stable set (of the 30th iterate) that contains the respective periodic point; see [6] for details. The bifurcation curves for the adaptive control example Fig. 6.2(a) were computed with the software package TBC [28]. Standard continuation techniques were used to compute the Neimark-Sacker and saddle-node bifurcation curves.

We focus in this section on the noninvertible bifurcation phenomena that we computed, namely, on the continuation of the curves of loop-creation bifurcation and cusp-transition bifurcation, and the detection of the codimension-two cusp-cusp point.

A.1. Abstract bifurcation conditions. For the endomorphism f we consider the Jacobian determinant function $J(x) = \det(Df(x))$. The critical curve J_0 is implicitly defined by $J_0 \equiv \{x \in \mathbb{R}^2 : J(x) = 0\}$; see (1.2). The tangent to J_0 at a point $x \in J_0$ is then given by $theperpendiculartothegradient, (\nabla J(\mathbf{x}))^{\perp}$. Thus, the defining

condition for C_0 to be a precusp point on J_0 is that

$$Df(C_0) \cdot (\nabla J(C_0))^{\perp} = \begin{pmatrix} 0 \\ 0 \end{pmatrix}. \tag{A.1}$$

To specify the interaction of J_0 with the unstable manifold we assume that $p \in \mathbb{R}^2$ is a saddle point of f (or of an appropriate iterate of f) and we let

$$\begin{aligned} \boldsymbol{\alpha} : [0, \infty) &\to \mathbb{R}^2 \\ t \quad &\mapsto \boldsymbol{\alpha}(t) \end{aligned}$$

be a parametrization of a branch of the unstable manifold $W^u(p)$, where $\boldsymbol{\alpha}(0) = p$. Furthermore, we assume that $W^u(p)$ intersects the critical curve J_0 at a point $\boldsymbol{\alpha}(t^*)$.

We can now formulate the *loop-creation condition* as

$$Df(\boldsymbol{\alpha}(t^*)) \cdot \boldsymbol{\alpha}'(t^*) = \begin{pmatrix} 0 \\ 0 \end{pmatrix}, \tag{A.2}$$

which ensures that $W^u(p)$ crosses J_0 tangent to the zero eigenvector, that is, the line field $\mathcal{E}$; see also Proposition 4.1.

Similarly, we formulate the *cusp-transition condition* as

$$Df(\boldsymbol{\alpha}(t^*)) \cdot (\nabla J(\boldsymbol{\alpha}(t^*)))^{\perp} = \begin{pmatrix} 0 \\ 0 \end{pmatrix}, \tag{A.3}$$

which ensures that the crossing point is exactly C_0.

At the codimension-two cusp-cusp point itself, both $\boldsymbol{\alpha}'(t^*)$ and $(\nabla J(\boldsymbol{\alpha}(t^*)))^{\perp}$ are zero eigenvectors, that is, both equations (A.2) and (A.3) must hold. However, requiring the latter as a condition for a cusp-cusp point turns out to be overdetermined. All we really need is either equation (A.2) or (A.3), along with ensuring the *parallel-vectors condition*

$$\boldsymbol{\alpha}'(t^*) \cdot \nabla J(\boldsymbol{\alpha}(t^*)) = 0. \tag{A.4}$$

A.2. Implementation. All three noninvertible bifurcations described above are implemented numerically by using Newton's method to solve a system of equations. We use the variables

$$\mathbf{x}_0, \mathbf{x}_1, ..., \mathbf{x}_k, \mu_1, \mu_2 \tag{A.5}$$

where the phase variables $\mathbf{x}_i \in \mathbb{R}^2$ and the parameters $\boldsymbol{\mu} = (\mu_1, \mu_2) \in \mathbb{R}^2$. In total these are $2k + 4$ scalar variables.

Each system of equations that we construct must, therefore, satisfy $2k + 4$ scalar equations. We first list the relevant equations.

1. The condition that $\mathbf{x}_0$ is a period-q point gives the two scalar equations:

$$f^q_{\boldsymbol{\mu}}(\mathbf{x}_0) - \mathbf{x}_0 = \mathbf{0} \tag{A.6}$$

2. We require that $\mathbf{x}_1$ be in the unstable eigenspace, which is the common approximation for the condition that $\mathbf{x}_1 \in W^u_{\text{loc}}(\mathbf{x}_0)$. This gives the single scalar equation

$$\frac{\mathbf{x}_1 - \mathbf{x}_0}{\|\mathbf{x}_1 - \mathbf{x}_0\|} \cdot \mathbf{v}^{\perp} = 0, \tag{A.7}$$

where $\mathbf{v}^{\perp}$ is a unit vector perpendicular to an unstable eigenvector $\mathbf{v}$ of $\mathbf{x}_0$.

3. The condition that $\mathbf{x}_1, ..., \mathbf{x}_k$ is an orbit for f_μ^q (which lies on $W^u_{\text{loc}}(\mathbf{x}_0)$ if $\mathbf{x}_1$ does) gives rise to the $2k-2$ scalar equations

$$f^q_{\boldsymbol{\mu}}(\mathbf{x}_i) - \mathbf{x}_{i+1} = \mathbf{0},\ i = 1, ..., k-1 \tag{A.8}$$

Note that q needs to be replaced here with $2q$ if the unstable eigenvalue is negative.

4. The condition $\mathbf{x}_k = C_0$ gives rise to the two scalar equations

$$Df^q_{\boldsymbol{\mu}}(\mathbf{x}_k) \cdot (\nabla(J_\mu(\mathbf{x}_k)))^\perp = \begin{pmatrix} 0 \\ 0 \end{pmatrix} \tag{A.9}$$

The partial derivatives in the gradient are computed using a forward difference quotient.

5. The condition that $W^u_{\text{loc}}(\mathbf{x}_0)$ undergoes a loop-creation associated with $\mathbf{x}_k$ gives rise to the two scalar equations

$$Df^q_{\boldsymbol{\mu}}(\mathbf{x}_k) \cdot \mathbf{t}_k = \begin{pmatrix} 0 \\ 0 \end{pmatrix}. \tag{A.10}$$

Here, the vector $\mathbf{t}_k = Df^{q(k-1)}(\mathbf{x}_1) \cdot (\mathbf{x}_1 - \mathbf{x}_0)/\|Df^{q(k-1)}(\mathbf{x}_1) \cdot (\mathbf{x}_1 - \mathbf{x}_0\|$ is an approximation to a unit tangent vector of the unstable manifold at $\mathbf{x}_k$. This equation is intended to be used with (A.7) so that $\mathbf{x}_1 - \mathbf{x}_0$ is an eigenvector at $\mathbf{x}_0$, and thus an approximation to a tangent vector to the unstable manifold at $\mathbf{x}_1$ *if* $\mathbf{x}_1$ is close to $\mathbf{x}_0$.

6. The condition that the tangent to $W^u_{\text{loc}}(\mathbf{x}_0)$ and the gradient of the Jacobian function are perpendicular gives rise to the single scalar equation

$$(\nabla(J_{\boldsymbol{\mu}}(\mathbf{x}_k))) \cdot \mathbf{t}_k = 0 \tag{A.11}$$

7. We also require the standard pseudo arclength continuation condition that convergence from the initial guess for Newton's method is perpendicular to the pseudo tangent $\mathbf{T}$ to the bifurcation curve being computed. This gives rise to the single scalar equation

$$\mathbf{T} \cdot ((\mathbf{x}_k, \mu_1, \mu_2) - (\mathbf{x}_k, \mu_1, \mu_2)_0) = 0. \tag{A.12}$$

Here we approximate the tangent vector $\mathbf{T}$ by the direction through the last two computed points. In our case, we project the tangent vector to the four-dimensional product of phase and parameter space, where $\mathbf{x}_k$ is considered to be the phase space 'representative' for the orbit; the zero subscript of the second tuple indicates that this is the initial guess provided to Newton's method.

For each of the three bifurcations from Sec. A.1 we require that the $2k+1$ equations (A.6), (A.7) and (A.8) are satisfied. Furthermore, these bifurcations are defined by additional requirements as follows.

- The codimension-one cusp-transition bifurcation is determined by equations (A.9) and (A.12),
- the codimension-one loop-creation bifurcation is determined by equations (A.10) and (A.12), and

- the codimension-two cusp-cusp point is determined by equation (A.11) along with either (A.9) or (A.10).

We implemented here only the above bifurcations, as this provides a convenient way of identifying the cusp-cusp point in a practical application. The formulation of conditions and, hence, numerical algorithms for the continuation of other bifurcations, in particualar, the intersection-at-tangency bifurcation, the tangency-creation bifurcation and the enter-exit bifurcation, could be developed within the framework presented here. However, this presents quite an interesting numerical challenge that is beyond the scope of this paper.